S©MR

СИБИРСКИЕ ЭЛЕКТРОННЫЕ
МАТЕМАТИЧЕСКИЕ ИЗВЕСТИЯ
Siberian Electronic Mathematical Reports
http://semr.math.nsc.ru
ISSN 1813-3304

Vol. 23, No. 1, pp. 449–483 (2026)
https://doi.org/10.33048/semi.2026.23.029

УДК 519.63
MSC 65M06, 65M12

ON THE ACCURACY OF SHOCK-CAPTURING SCHEMES INSIDE VARIOUS SMOOTHNESS REGIONS OF THE APPROXIMATED WEAK SOLUTIONS

O.A. KOVYRKINA, **V.V. OSTAPENKO**

Communicated by M.A. Shishlenin

Abstract: We study the accuracy of shock-capturing schemes for hyperbolic systems of conservation laws theoretically and numerically. Based on the method of differential approximation of the numerical schemes, we give a theoretical justification for the fact that high order shock-capturing schemes can have significantly different accuracy in the various smoothness regions of calculated weak solutions. We also show that in the case of the hyperbolic system with invariants, different invariants of this system can be calculated with significantly different accuracy in the same smoothness region of the exact solution, in particular, in the shock influence areas or inside the centered rarefaction waves. To illustrate these theoretical results, we use test calculations by the RBM (Rusanov-Burstein-Mirin), TVD and WENO5 finite-difference schemes of the special shallow water Cauchy problem, which exact solution contains a shock and centered rarefaction waves.

Keywords: finite-difference schemes, shock-capturing schemes, high accuracy, order reduction behind the shocks, pointwise convergence

Kovyrkina, O.A., Ostapenko, V.V. On the accuracy of shock-capturing schemes inside various smoothness regions of the approximated weak solutions.

The reported study was partially funded by the Russian Science Foundation (project no. 22-11-00060) Sections 4–5.

Received July, 11, 2025, Published May, 18, 2026.

1 Introduction

In classical paper [1] associated with an original numerical technique for Riemann solver, Godunov introduced the concept of a monotone numerical scheme and proved that, among the linear two-layer in time schemes, there are no monotone ones with an order of accuracy higher than the first. The subsequent development of the theory of shock-capturing schemes for hyperbolic systems of conservation laws was aimed to a large degree at the overcoming of the Godunov order barrier. As a result, various classes of finite-difference, finite-volume and projection shock-capturing schemes were developed in which a high order of accuracy for smooth solutions and monotonicity (in the approximation of linear systems and scalar conservation laws) were achieved by applying Nonlinear Flux Correction (NFC), which leads to the nonlinearity of these schemes even in the approximation of the linear equations. The following papers underlie whole classes of the NFC schemes: MUSCL [2], TVD [3], ENO [4], NT [5], WENO [6, 7], DG [8], CU [9, 10] and CABARET [11]. The NFC schemes also include hybrid schemes [12, 13, 14, 15] in which the numerical solution is monotonized using a special numerical algorithm in the vicinity of large gradients of the exact solution. Various methods for constructing the NFC schemes and their practical application are described in [16, 17, 18, 19] and references therein. The advantage of these schemes is they localizing shocks with high accuracy in the absence of considerable spurious oscillations. However, it was shown in [20, 21, 22] that the NFC schemes of different types have at most the first convergence order in the post shock areas regardless of their accuracy on smooth solutions.

To more detailed study the accuracy of shock-capturing schemes inside the shock influence domains, we proposed [23] for the shallow water system [24]

$$H_t + q_x = 0, \quad q_t + \left(q^2/H + gH^2/2\right)_x = 0 \tag{1}$$

the special Cauchy problem with smooth periodic initial data of invariants $w_1 = u - 2c$ and $w_2 = u + 2c$:

$$w_1(x,0) = -10, \quad w_2(x,0) = 4\sin\left(\frac{2\pi x}{X} + \frac{\pi}{4}\right) + 10, \tag{2}$$

where $H(x,t)$, $q(x,t)$, $u = q/H$, $c = \sqrt{gH}$, $g = 9.81$ and $X = 10$ are the depth, the fluid flow rate, the horizontal fluid velocity, the velocity of small disturbances propagation, the gravity acceleration and the period length, respectively. For such problem, we will use an abbreviation SPC (Special Periodic Cauchy).

In the exact solution of the SPC problem, at the time moment $t^* \approx 0.54$, as a result of gradient catastrophes, a sequence of isolated shocks $x = s_i(t)$ is formed, which propagate one after another at the same distance X and with the same positive velocities (Fig. 1). Since these shocks initially (at $t = t^* + 0$) appear as strong discontinuities of infinitesimal amplitude, the

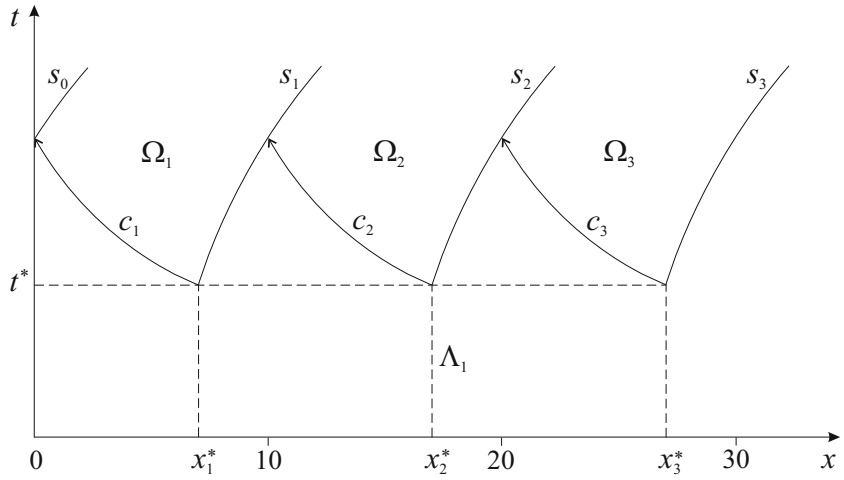

FIGURE 1. Shock waves s_i and different smoothness regions Λ_1, Ω_i of the exact solution.

exact solution of the SPC problem in the area

$$\Lambda = \{(x,t): \quad t \geq 0; \quad x \neq s_i(t),\ t \geq t^*,\ i \in \mathbb{Z}\} \tag{3}$$

is quite smooth, where $\mathbb{Z}$ is the set of integers. Despite this, numerical calculations of the SPC problem using various high order shock-capturing schemes have shown [23, 25, 26, 27, 28, 29, 30, 31, 32, 33] that these schemes have significantly different accuracy in the regions $\Lambda_1 \in \Lambda$ and $\Lambda_2 = \Lambda \backslash \Lambda_1$, where Λ_1 is the region of smoothness of the exact solution that does not intersect with the shock influence domains,

$$\Lambda_2 = \bigcup_{i \in \mathbb{Z}} \Omega_i, \tag{4}$$
$$\Omega_i = \{(x,t): \ \max\left(s_{i-1}(t), c_i(t)\right) < x < s_i(t),\ t \geq t^*\},$$

is the set of shock influence domains (Fig. 1), located between neighboring shocks, where $x = c_i(t)$ is the characteristic propagating with the velocity $\lambda_1 = u - c$ across the i-th point of the gradient catastrophe (x_i^*, t^*), $x_i^* = s_i(t^*)$.

Calculations have shown that in the region Λ_1 each of the considered schemes has the convergence order that coincides with its approximation order on smooth solutions. It is consistent with approximately identical accuracy of the invariants calculation in this region, which increases with scheme order increasing. The situation is fundamentally different in the shock influence domains Ω_i, where the convergence orders of all schemes become smaller than their formal approximation orders and the invariant w_1 is calculated with a much lower accuracy than the invariant w_2. For a more detailed analysis of this situation it was proposed [23] to investigate

the convergence order of the numerical values of the integrals

$$\boldsymbol{U}(a,b,t)=\int\limits_a^b \boldsymbol{u}(x,t)dx, \quad \boldsymbol{u}=\begin{pmatrix} H \\ q \end{pmatrix},$$

calculated by high-precision integro-interpolation formula on intervals $[(a,t),(b,t)]$ with one or both endpoints are inside the shock influence domains (4); for such convergence, following [32], we will use an abbreviation NINSID (Negative Integral Norm Shock Influence Domain). It is shown [23, 25, 26, 30, 31, 32, 33] that when calculating the SPC problem by the NFC schemes, they have only the first order of the NINSID convergence (regardless of their formal orders on smooth solutions), which leads to a corresponding decrease in the accuracy of the NFC schemes in the shock influence domains.

The shock-capturing schemes that do not belong to the NFC type and become linear when applied to a linear approximation of a quasilinear hyperbolic system we will designate QL (Quasi-Linear) schemes. It was shown in [23, 27, 28, 29, 32, 33] that some high order QL schemes, in particular, the RBM scheme [34, 35], have the second order of the NINSID convergence in the numerical calculations of the SPC problem and as a result, unlike the NFC schemes, these schemes maintain an increased accuracy inside the shock influence domains (4), despite noticeable scheme oscillations at the shocks. In [32] for such QL schemes a special abbreviation HASIA (High Accuracy Shock Influence Area) was introduced. The reason of this was follows. When calculating the SPC problem, some high-order QL schemes, for example, the Lax-Wendroff scheme [36], just like the NFC schemes, have the first order of the NINSID convergence, so these schemes lose increased accuracy inside the shock influence domains. The existence of the HASIA schemes predetermined the possibility of constructing combined shock-capturing schemes [27, 28, 29, 32, 33] that unites the advantages of the NFC and HASIA schemes: combined schemes monotonically localize shocks and simultaneously keep an increased accuracy in the shock influence domains.

The main purpose of this paper is to offer a theoretical justification for the numerical results mentioned above. In Section 2 we formulate the Cauchy problem for a hyperbolic system of conservation laws and give a brief description of three high order shock-capturing schemes approximating this problem, namely, the HASIA RBM scheme [34] and also the NFC schemes TVD [3] and WENO5 [7]. In Section 3 the Runge formula is presented, which is used to approximate calculations of the local convergence orders of numerical solutions. In the theoretical Section 4, the hyperbolic systems of differential equations are obtained for the approximate determination of the disbalances (errors) of the numerical solution in various continuity regions of the calculated exact solution. An important feature of these systems is that its characteristics field coincides with the characteristics field of the approximated system of conservation laws, which determines to a significant

extent the scheme accuracy inside corresponding continuity region of the approximated weak solution.

An analysis of internal initial-boundary value problems arising in the exact solution continuity regions for hyperbolic numerical disbalance systems allows us to give a theoretical justification for the fact that high order shock-capturing schemes can have significantly different accuracy in the different continuity regions of calculated weak solutions. We also analytically showed that in the case of the hyperbolic system with invariants, different invariants of this system can be calculated with significantly different accuracy in the same continuity region of the exact solution, in particular, in the shock influence areas or inside the centered rarefaction waves. To illustrate these theoretical results in Section 5, we use test calculations by the RBM, TVD and WENO5 finite-difference schemes of the special shallow water Cauchy problems, which exact solutions contains a shock and centered rarefaction wave.

In the final Section 6 we give a general description of the results and formulate the main promising directions for further development of the combined scheme theory.

2 Considered shock-capturing schemes approximating the hyperbolic system of conservation laws

Let us consider a hyperbolic system of conservation laws

$$\boldsymbol{u}_t + \boldsymbol{f}(\boldsymbol{u})_x = 0, \tag{5}$$

where $\boldsymbol{u}(x,t)$ is unknown vector function and $\boldsymbol{f}(\boldsymbol{u})$ is given smooth vector function containing m components. For system (5), we set the Cauchy problem with an initial data

$$\boldsymbol{u}(x,0) = \boldsymbol{u}_0(x), \tag{6}$$

where $\boldsymbol{u}_0(x)$ is given bounded function. We will assume that the problem (5), (6) has a unique weak solution $\boldsymbol{u}(x,t)$ in the class of piecewise smooth bounded functions with shocks.

Explicit numerical schemes approximating problem (5), (6) will be constructed on a rectangular uniform grid

$$S = \{(x_j, t_n) : \ x_j = jh, \ t_n = n\tau, \quad n \geq 0\}, \tag{7}$$

where h and $\tau = rh$ are constant grid steps in space and time, r is a parameter that we choose taking into account the CFL stability condition

$$\theta = \frac{\tau}{h} = \frac{z}{\max\limits_{i,j,n} |\lambda_i(\boldsymbol{v}_j^n)|}, \quad z \in (0,1), \tag{8}$$

where $\lambda_i(\boldsymbol{u})$ is the Jacobian eigenvalues of system (5) and $\boldsymbol{v}_j^n = \boldsymbol{v}_h(x_j, t_n)$ is a numerical solution. When performing applied calculations, to save computer time, a time-nonuniform numerical grid is usually used

$$\widetilde{S} = \{(x_j, t_n) : \ x_j = jh, \ t_{n+1} = t_n + \tau_n, \ t_0 = 0\},$$

where the variable time step τ_n is determined by the formula

$$\tau_n = \frac{zh}{\max\limits_{i,j} |\lambda_i \left(\boldsymbol{v}_j^n \right)|}, \quad z \in (0,1).$$

However, for the purposes of this paper related to the experimental study of the scheme accuracy on a sequence of imbedded grids, it is more natural to use uniform numerical grids (7) with a constant time step given by the formula (8).

Let us consider the following shock-capturing finite-difference schemes, approximating the Cauchy problem (5), (6): the third order RBM scheme [34, 35], the second order TVD scheme [3] and the fifth-order in space and the third order in time WENO5 scheme [7]. The RBM scheme belongs to the class of the HASIA schemes, while the TVD and WENO5 belong to the class of the NFC schemes. Let us give a brief description of these schemes.

The RBM scheme was the first scheme of the third order in which the three-step Runge-Kutta method was used for time approximation; brief information about this scheme was published in [34], its detailed analysis was performed in [35]. To ensure numerical stability in the RBM scheme, a special artificial viscosity was used, which is a fourth-order divergence difference operator approximating the fourth spatial derivative; the coefficient C of this viscosity should satisfy the inequalities

$$3 \geq C \geq z^2(4 - z^2).$$

Test calculations of discontinuous solutions of the gas dynamic equations were performed at close values of $C = 2.5$ in [34] and $C = 2.8$ in [35]. In the present paper we use the value $C = 2.5$.

In classical paper [3], the TVD property of the difference scheme was introduced, which assumes that when calculating the Cauchy problem for a scalar conservation law, the total variation of the difference solution does not increase when moving from one time layer to another, which corresponds to a similar property of the exact solution [37]. The Harten TVD property is equivalent to the Godunov monotonicity property [1] when approximating linear equations and enhances the monotonicity property when approximating a quasilinear scalar conservation law [38]. The TVD scheme is constructed by monotonizing the Lax-Wendroff scheme [36] and is an explicit two-layer in time difference scheme, in which the numerical fluxes are corrected as a result of applying a special minimax procedure, which reduces their smoothness to the level of Lipschitz-continuous functions. For a small heuristic parameter included in this correction procedure, we take the value $\varepsilon = 0.1$ offered in [3], which ensures the decay of unstable strong discontinuities that the Lax-Wendroff scheme can admit [39]. With this ε value, the TVD scheme is strongly monotonic [40], that is similar to the fulfillment of the NED property [41]. If the approximated hyperbolic system (5) has a convex extension [42], the selection of stable shocks in the TVD scheme

occurs due to the difference analogue of the entropy inequality. When calculating smooth solutions, the TVD scheme has the second order of accuracy everywhere except the local extrema of these solutions, where it has the first order of convergence.

The WENO schemes [6, 7] are based on the ENO schemes [4, 43], in which TVD property [3] holds approximately. The key idea of the ENO schemes, associated with choosing the most "smoothest" stencil among several candidates to approximate the fluxes, in the WENO schemes is modified as follows: one uses a convex combination of all the candidate stencils and each of the stencils is assigned a weight which determines its contribution to the final approximation of the numerical flux. We will apply the fifth order in space and the third order in time WENO5 scheme [7], which uses global Lax-Fridrichs flux spliting for spatial approximation and three-step Runge-Kutta method for time approximation. For a small heuristic parameter included in this scheme, we take the value $\varepsilon = 10^{-6}$. In contrast to the TVD scheme, the WENO5 scheme preserves increased accuracy at the local extrema of the calculated smooth solutions. In addition, in contrast to other classes of the NFC schemes, in which different types of minimax flux corrections are used to monotonize the difference solution, in the WENO schemes such a correction is achieved by introducing weight parameters, which allows maintaining the increased smoothness of the numerical flux functions.

3 Methods for estimating the accuracy of numerical solutions

To estimate the local convergence orders of the numerical solution $\boldsymbol{v}_j^n = \boldsymbol{v}_h(x_j, t_n)$, given on the uniform grid (3), we fix on this grid some node (x_j, t_n), where $n \geq 1$, and introduce for it a new notation (x_*, t_*), where $x_* = jh$ and $t_* = n\tau > 0$. Suppose that on a sequence of imbedded grids

$$S_i = \{(x_j^i, t_n^i) : \ x_j^i = jh_i, \ t_n^i = n\tau_i, \ n \geq 0\}, \quad i = 1, 2, \ldots, \tag{9}$$

where $h_i = h/2^{i-1}$ and $\tau_i = \tau/2^{i-1}$, which is based on the basic grid (3), the numerical solution $\boldsymbol{v}_{h_i}$ converges with order r to the exact solution $\boldsymbol{u}$ at the point (x_*, t_*). This means that at this point, with accuracy $o(h_i^r)$, condition

$$\boldsymbol{v}_{h_i} - \boldsymbol{u} = \boldsymbol{C} h_i^r \tag{10}$$

is satisfied, where $\boldsymbol{C}$ is a vector quantity independent of h_i and such that $|\boldsymbol{C}| > 0$.

Since in the general case the exact solution $\boldsymbol{u}$ is unknown, to estimate the convergence order r we will use Runge method [32]. Subtracting from formula (10) the same formula, in which the index i is replaced by $i+1$, we obtain

$$\boldsymbol{v}_{h_i} - \boldsymbol{v}_{h_{i+1}} = \boldsymbol{C}\left(h_i^r - h_{i+1}^r\right) \ \Rightarrow \ |\boldsymbol{v}_{h_i} - \boldsymbol{v}_{h_{i+1}}| = |\boldsymbol{C}|\, h_i^r \left(1 - 2^{-r}\right). \tag{11}$$

Taking the ratio of the second equalities (11) for $i = 1, 2$, we have

$$\frac{|\boldsymbol{v}_{h_1} - \boldsymbol{v}_{h_2}|}{|\boldsymbol{v}_{h_2} - \boldsymbol{v}_{h_3}|} = \left(\frac{h_1}{h_2}\right)^r = 2^r.$$

This implies the Runge formula

$$r = \log_2 \frac{|\boldsymbol{v}_{h_1} - \boldsymbol{v}_{h_2}|}{|\boldsymbol{v}_{h_2} - \boldsymbol{v}_{h_3}|} = \log_{1/2} \frac{|\boldsymbol{v}_{h_2} - \boldsymbol{v}_{h_3}|}{|\boldsymbol{v}_{h_1} - \boldsymbol{v}_{h_2}|} \tag{12}$$

for determining the local convergence orders of the numerical solution to the exact one.

Since the first equation (11) for $i = 1$ is written in the form

$$\boldsymbol{v}_{h_1} - \boldsymbol{v}_{h_2} = \boldsymbol{C}\left(h_1^r - h_2^r\right) = \boldsymbol{C}h^r\left(1 - 2^{-r}\right),$$

the vector $\boldsymbol{C}$ can be represented as follows

$$\boldsymbol{C} = \frac{\boldsymbol{v}_{h_1} - \boldsymbol{v}_{h_2}}{h^r\left(1 - 2^{-r}\right)}. \tag{13}$$

Substituting the value (13) in formula (10), for $i = 1$ we obtain

$$\boldsymbol{v}_h - \boldsymbol{u} = \boldsymbol{v}_{h_1} - \boldsymbol{u} = \frac{\boldsymbol{v}_{h_1} - \boldsymbol{v}_{h_2}}{1 - 2^{-r}}.$$

Hence, taking into account (12) we have the formula

$$\delta\boldsymbol{v}_h = \boldsymbol{v}_h - \boldsymbol{u} = (\boldsymbol{v}_{h_1} - \boldsymbol{v}_{h_2})\left(1 - \frac{|\boldsymbol{v}_{h_2} - \boldsymbol{v}_{h_3}|}{|\boldsymbol{v}_{h_1} - \boldsymbol{v}_{h_2}|}\right)^{-1} \tag{14}$$

for an approximate estimate of the error of the vector numerical solution on the base grid (7).

Let us consider some smooth scalar function $w = w(\boldsymbol{u})$ of the vector solution $\boldsymbol{u}$, and we have to estimate the accuracy of calculation for it. Suppose that on the sequence of imbedded grids (9) the numerical function $w_{h_i} = w(\boldsymbol{v}_{h_i})$ at the point (x_*, t_*) converges with the order ρ to the exact function $w = w(\boldsymbol{u})$. This means that at this point, with accuracy $o(h_i^\rho)$, condition

$$w_{h_i} - w = Bh_i^\rho \tag{15}$$

is satisfied, where B is a scalar quantity independent of h_i and such that $B \neq 0$. If the calculated solution $\boldsymbol{u}$ is smooth, the vector and scalar convergence orders r and ρ is equal to each other ($r = \rho$) for any smooth function $w = w(\boldsymbol{u})$. At the same time, if the exact solution $\boldsymbol{u}$ is not smoth and contains shocks or centered rarefaction waves, then in the shock influence domain and inside centered rarefaction waves for some functions $w(\boldsymbol{u})$, in particular, for invariants of the exact solution, vector and scalar convergence orders can be different ($r \neq \rho$). Taking this into account, to estimate the scalar convergence order ρ we will use formula

$$\rho = \log_2 \frac{|w_{h_1} - w_{h_2}|}{|w_{h_2} - w_{h_3}|} = \log_{1/2} \frac{|w_{h_2} - w_{h_3}|}{|w_{h_1} - w_{h_2}|} \tag{16}$$

and to estimate the error in calculation of the function $w(\boldsymbol{u})$ we will apply the formula

$$\delta w_h = w_h - w = (w_{h_1} - w_{h_2}) \left(1 - \frac{|w_{h_2} - w_{h_3}|}{|w_{h_1} - w_{h_2}|}\right)^{-1}. \tag{17}$$

Formulas (16) and (17) are derived from condition (15) in the same way as formulas (12) and (14) are derived from condition (10).

If the local convergence orders $r = r_h(x_j, t_n)$ and $\rho = \rho_h(x_j, t_n)$ defined by formulas (12) and (16) oscillate sharp at time t_n, we will show in figures the averaged local convergence orders bounded above

$$\begin{aligned} \bar{r} = \bar{r}_h(x_j, t_n) &= \begin{cases} \hat{r}(x_j, t_n), & \hat{r}(x_j, t_n) \le 4, \\ 4, & \hat{r}(x_j, t_n) > 4, \end{cases} \\ \bar{\rho} = \bar{\rho}_h(x_j, t_n) &= \begin{cases} \hat{\rho}(x_j, t_n), & \hat{\rho}(x_j, t_n) \le 4, \\ 4, & \hat{\rho}(x_j, t_n) > 4, \end{cases} \end{aligned} \tag{18}$$

where

$$\hat{r}_h(x_j, t_n) = \frac{1}{15} \sum_{i=-7}^{7} r_h(x_{j+i}, t_n), \quad \hat{\rho}_h(x_j, t_n) = \frac{1}{15} \sum_{i=-7}^{7} \rho_h(x_{j+i}, t_n),$$

calculated on the sufficiently fine basic grid (7). In the figures we will also show relative errors of numerical solution, determined by the formulas

$$\Delta \boldsymbol{v}_h = \lg \frac{|\delta \boldsymbol{v}_h|}{|\boldsymbol{v}_h|}, \quad \Delta w_h = \lg \frac{|\delta w_h|}{|w_h|}. \tag{19}$$

4 Disbalances of the difference solution in the continuity regions of calculated weak solution

In this section, we will compare the dependence regions of the exact and numerical solutions of the Cauchy problem (5), (6), will obtaine a hyperbolic systems of differential equations for the approximate determination of disbalances (errors) of the numerical solution in continuity regions of the calculated weak solution. Using these systems, we will justify that high order shock-capturing schemes can have significantly different accuracy in the various regions of such type, and in the case of the hyperbolic system (5) with invariants, we will show that different invariants of this system can be calculated with significantly different accuracy in the same continuity region of the exact solution.

4.1. Dependency domain of the exact and numerical solutions. Since the considered finite difference schemes RBM, TVD and WENO5 are conservative, explicit and two-layer in time, they can be written in the following divergent form

$$\frac{\boldsymbol{v}_j^{n+1} - \boldsymbol{v}_j^n}{\tau} + \frac{\bar{\boldsymbol{f}}_{j+1/2}^n - \bar{\boldsymbol{f}}_{j-1/2}^n}{h} = 0, \tag{20}$$

where the numerical fluxes $\bar{\boldsymbol{f}}^n_{j\pm1/2}$ is determined by the formulas

$$\begin{aligned}\bar{\boldsymbol{f}}^n_{j+1/2} &= \bar{\boldsymbol{f}}\left(\boldsymbol{v}^n_{j-l+1}, \boldsymbol{v}^n_{j-l+2}, \ldots, \boldsymbol{v}^n_{j+l}, \theta\right),\\ \bar{\boldsymbol{f}}^n_{j-1/2} &= \bar{\boldsymbol{f}}\left(\boldsymbol{v}^n_{j-l}, \boldsymbol{v}^n_{j-l+1}, \ldots, \boldsymbol{v}^n_{j+l-1}, \theta\right),\end{aligned} \tag{21}$$

in which $l = 2$ for the RBM and TVD schemes, and $l = 9$ for the WENO5 scheme. Numerical fluxes (21) are consistent with the differential flux $\boldsymbol{f}(\boldsymbol{u})$ of the system (5) in the sense of fulfilling relation

$$\bar{\boldsymbol{f}}(\boldsymbol{u}, \ldots, \boldsymbol{u}, r) = \boldsymbol{f}(\boldsymbol{u}). \tag{22}$$

Let us denote by $M[\boldsymbol{u}_0]$ the set of points of strong discontinuities for the initial function $\boldsymbol{u}_0(x)$, which is used in the formulation of the Cauchy problem (6) for the hyperbolic system (5). In the calculations below, the discontinuous initial data (6) and the numerical grid (7) are chosen in such a way that all points of the set $M[\boldsymbol{u}_0]$ are integer nodes x_j of the numerical grid (7). Taking this into account, for the considered numerical schemes, the approximation of the initial data (6) at integer grid nodes is given by the formula

$$\boldsymbol{v}^0_j = \boldsymbol{v}_h(x_j, 0) = \begin{cases} \boldsymbol{u}_0(x_j), & x_j \notin M[\boldsymbol{u}_0],\\ \dfrac{1}{2}\left(\boldsymbol{u}_0(x_j - 0) + \boldsymbol{u}_0(x_j + 0)\right), & x_j \in M[\boldsymbol{u}_0]. \end{cases} \tag{23}$$

As shown in [36], the bounded discontinuous solution of the finite-difference initial problem (20)–(23) is weak solution $\boldsymbol{u}(x,t)$ of the approximated differential Cauchy problem (5), (6).

From formulas (20) and (21) it follows that the resulting difference solution $\boldsymbol{v}^n_j = \boldsymbol{v}(x_j, t_n)$ at a fixed node (x_j, t_n), where $n \geq 1$, depends on its values at the grid nodes, which at each time level k, where $0 \leq k \leq n-1$, form a finite set

$$P_k(x_j, t_n) = \{(x_{j+i}, t_k) :\ i = -sl, \ldots, sl,\ s = n - k\}. \tag{24}$$

Union of sets (24)

$$V(x_j, t_n) = \bigcup_{k=0}^{n-1} P_k(x_j, t_n) \tag{25}$$

is the dependence domain of the numerical solution of the grid Cauchy problem (20)–(23) at the node (x_j, t_n).

Let us fix the point (x_*, t_*), where $x_* = jh$, $t_* = n\tau > 0$ and for each grid S_i included in the sequence (9) construct the dependence domain of type (25) at the point (x_*, t_*); for this domain we will use the notation $V_i(x_*, t_*)$, where $V_1(x_*, t_*) = V(x_*, t_*)$. The limiting discrete set

$$V_{\lim}(x_*, t_*) = \lim_{i \to +\infty} V_i(x_*, t_*)$$

everywhere densely fills the triangular region

$$\begin{aligned}V_{\text{num}}(x_*, t_*) &=\\ &= \{(x,t) :\ L_-(t, x_*, t_*) \leq x \leq L_+(t, x_*, t_*),\ 0 \leq t \leq t_*\},\end{aligned} \tag{26}$$

where, taking into account the stability condition (8),

$$L_{\pm}(t, x_*, t_*) = x_* \pm l\mu(t_* - t)/z, \quad \mu = \max_{i,x,t} |\lambda_i(\boldsymbol{u}(x,t))|, \tag{27}$$

$\boldsymbol{u}(x,t)$ is the approximated exact solution.

The triangular region (26) will be called the continual dependence set of the numerical solution at the point (x_*, t_*). By virtue of the CFL correctness condition [44], which is typical for the explicit finite-difference schemes, the continual dependence set (26) of their numerical solutions contains the dependence set

$$V_{\text{ex}}(x_*, t_*) = \\ = \{(x,t):\ L_m(t, x_*, t_*) \le x \le L_1(t, x_*, t_*),\ 0 \le t \le t_*\} \tag{28}$$

of the exact solution of the approximated differential problem (5), (6), i. e.

$$V_{\text{ex}}(x_*, t_*) \subseteq V_{\text{num}}(x_*, t_*), \tag{29}$$

where $x = L_i(t, x_*, t_*)$ is characteristic of the i-th family of the exact solution $\boldsymbol{u}$ coming at the point (x_*, t_*). Taking into account the stability condition (8), the RBM, TVD and WENO5 schemes satisfy the correctness condition (29); moreover, the WENO5 scheme has a large stencil, since the spatial size of its dependence region (26), determined by the number $l = 9$ included in the formula (27), significantly exceeds the spatial size of the dependence region (28) of the approximated exact solution.

4.2. Systems of equations for disbalances of a numerical solution. Suppose that finite-difference scheme (20) with k-th order approximates hyperbolic system (5). According to the CFL stability condition (8)

$$\tau = \theta h, \quad \theta = \text{const},$$

and this means that for each sufficiently smooth solution $\boldsymbol{u}(x,t)$ of the system (5) up to $o(h^k)$ we have

$$\boldsymbol{\Lambda}_h[\boldsymbol{u}(x,t)] = h^k \boldsymbol{\Phi}[\boldsymbol{u}(x,t)], \tag{30}$$

where $\boldsymbol{\Lambda}_h$ is the operator of the scheme

$$\begin{aligned} \boldsymbol{\Lambda}_h[\boldsymbol{w}_h(x,t)] = &\frac{\boldsymbol{w}_h(x, t+\tau) - \boldsymbol{w}_h(x,t)}{\tau} + \\ &+ \frac{\bar{\boldsymbol{f}}[\boldsymbol{w}_h(x+h/2,t)] - \bar{\boldsymbol{f}}[\boldsymbol{w}_h(x-h/2,t)]}{h} = 0, \end{aligned} \tag{31}$$

$$\bar{\boldsymbol{f}}[\boldsymbol{w}_h(x+h/2,t)] = \\ = \bar{\boldsymbol{f}}\left(\boldsymbol{w}_h(x-(l-1)h,t), \boldsymbol{w}_h(x-(l-2)h,t), \ldots, \boldsymbol{w}_h(x+lh,t), \theta\right),$$

$$\bar{\boldsymbol{f}}[\boldsymbol{w}_h(x-h/2,t)] = \\ = \bar{\boldsymbol{f}}\left(\boldsymbol{w}_h(x-lh,t), \boldsymbol{w}_h(x-(l-1)h,t), \ldots, \boldsymbol{w}_h(x+(l-1)h,t), \theta\right),$$

obtained from the finite-difference scheme (20) as a result of replacing the grid functions

$$\boldsymbol{v}_j^{n+1} = \boldsymbol{v}(x_j, t_n + \tau), \quad \boldsymbol{v}_{j+l}^n = \boldsymbol{v}(x_j + lh, t_n)$$

with functions $\boldsymbol{w}_h(x, t+\tau)$ and $\boldsymbol{w}_h(x+lh, t)$, depending on continuously changing arguments x and t; $\boldsymbol{\Phi}[\boldsymbol{u}(x,t)]$ is a vector differential operator depending on the function $\boldsymbol{u}(x,t)$ and its partial derivatives with respect to x up to $(k+1)$-th inclusive.

Since finite-difference scheme (20) is explicit and two-layer in time, the increased approximation order (30), where $k \geq 2$ is achieved due to the vector equation (5) and its differential consequences

$$\frac{\partial^s \boldsymbol{u}}{\partial t^l \partial x^{s-l}} + \frac{\partial^s \boldsymbol{f}(\boldsymbol{u})}{\partial t^{l-1} \partial x^{s-l+1}} = 0, \quad l = \overline{1, s}, \ s = \overline{2, k}. \tag{32}$$

The fulfillment of condition (30) implies not only the smoothness of the exact solution $\boldsymbol{u}(x,t)$ of approximated system (5), but also the corresponding smoothness of the numerical flux function $\bar{\boldsymbol{f}}$ of the scheme (20). The flux function $\bar{\boldsymbol{f}}$ in the RBM scheme is analytical and therefore this scheme has the third order of approximation. At the same time, the approximation order (30) for the TVD and WENO5 schemes can significantly depend on the smoothness of their numerical flux functions (21), which changes as a result of nonlinear flux correction. Taking this into account, in the general case, $k \leq 2$ for the TVD scheme and $k \leq 3$ for the WENO5 scheme.

Since sufficiently smooth solutions $\boldsymbol{w}_h(x,t)$ of the scheme (31) approximately satisfy the vector equation (5) and its differential consequences (32), this scheme on such solutions up to $o(h^k)$ can be represented in the form

$$(\boldsymbol{w}_h)_t + \boldsymbol{f}(\boldsymbol{w}_h)_x = h^k \boldsymbol{\Psi}[\boldsymbol{w}_h], \tag{33}$$

where $\boldsymbol{\Psi}[\boldsymbol{w}_h]$ is a vector differential operator depending on the function $\boldsymbol{w}_h(x,t)$ and its partial derivatives with respect to x up to $(k+1)$-th inclusive. The system (33), called in [45] the P-form of the First Differential Approximation (PFDA) of the finite-difference scheme (20), makes it possible to approximately simulate the behavior of the numerical solution $\boldsymbol{v}_j^n = \boldsymbol{v}(x_j, t_n)$ of this scheme in the smooth parts of the calculated weak solution $\boldsymbol{u}(x,t)$ of the Cauchy problem (5), (6).

Slightly modifying the method proposed in [46], we will construct a solution of the system (33) as the following series

$$\boldsymbol{w}_h(x,t) = \boldsymbol{u}(x,t) + \sum_{i=1}^{k} h^i \boldsymbol{w}_i(x,t) + o(h^k), \tag{34}$$

where $\boldsymbol{u}(x,t)$ is the smooth solution of the system (5). Substituting formula (34) in equation (33), taking into account the system (5), up to $o(h^k)$

we obtain

$$\sum_{i=1}^{k} h^i \left((\boldsymbol{w}_i)_t + (A(\boldsymbol{u})\boldsymbol{w}_i)_x\right) + \\ + \sum_{i=2}^{k} h^i \left(\boldsymbol{\Psi}_i(\boldsymbol{u}, \boldsymbol{w}_1, \boldsymbol{w}_2, \ldots, \boldsymbol{w}_{i-1})\right)_x = h^k \boldsymbol{\Psi}[\boldsymbol{u}], \quad (35)$$

where $A(\boldsymbol{u}) = \boldsymbol{f}_{\boldsymbol{u}}(\boldsymbol{u})$ is the Jacobian of the system (5), and $\boldsymbol{\Psi}_i$ are vector functions whose components are polynomials of the components of vector functions $\boldsymbol{w}_1, \boldsymbol{w}_2, \ldots, \boldsymbol{w}_{i-1}$; moreover, functions $\boldsymbol{\Psi}_i$ take zero values if all functions $\boldsymbol{w}_l$ included in them are zero, i.e.

$$\boldsymbol{\Psi}_i(\boldsymbol{u}, 0, 0, \ldots, 0) = 0, \quad i = \overline{2, k}. \quad (36)$$

Equating to zero the sums of coefficients at the same powers of h in equation (35), we obtain the following recurrent system of vector linear differential equations for functions $\boldsymbol{w}_i$ included in series (34):

$$(\boldsymbol{w}_1)_t + (A(\boldsymbol{u})\boldsymbol{w}_1)_x = 0, \quad (37)$$

$$(\boldsymbol{w}_i)_t + (A(\boldsymbol{u})\boldsymbol{w}_i)_x + \left(\boldsymbol{\Psi}_i(\boldsymbol{u}, \boldsymbol{w}_1, \boldsymbol{w}_2, \ldots, \boldsymbol{w}_{i-1})\right)_x = 0, \\ i = \overline{2, k-1}, \quad (38)$$

$$(\boldsymbol{w}_k)_t + (A(\boldsymbol{u})\boldsymbol{w}_k)_x + \left(\boldsymbol{\Psi}_i(\boldsymbol{u}, \boldsymbol{w}_1, \boldsymbol{w}_2, \ldots, \boldsymbol{w}_{k-1})\right)_x = \boldsymbol{\Psi}[\boldsymbol{u}]. \quad (39)$$

Since the matrix $A(\boldsymbol{u})$ in the systems (37)–(39) is the Jacobian of the approximated system (5), the systems (37)–(39) are hyperbolic and their characteristics fields coincide with the characteristics field of system (5).

We fix some point (x_*, t_*) with $t_* > 0$ and at first assume that weak solution $\boldsymbol{u}(x, t)$ of the Cauchy problem (5), (6) is smooth in the dependence set (28). In this case, the solution of system (37)–(39) at the point (x_*, t_*) can be obtained if for the functions $\boldsymbol{v}_i$ the initial conditions are set on interval

$$I = \{x : \ (x, 0) \in V_{\text{ex}}(x_*, t_*)\}. \quad (40)$$

Since numerical initial data (23) on continuity interval (40) of the initial function $\boldsymbol{u}_0(x)$ correspond to the initial conditions

$$\boldsymbol{w}_h(x, 0) = \boldsymbol{u}_0(x), \quad x \in I, \quad (41)$$

for scheme (31) and its PFDA (33), substituting conditions (41) in formula (34), written at $t = 0$, and taking into account (6), we obtain

$$\boldsymbol{w}_i(x, 0) = 0, \quad x \in I, \quad i = \overline{1, k}. \quad (42)$$

According to relations (36), homogeneous equations (37) and (38) with initial conditions (42) have zero solutions

$$\boldsymbol{w}_i(x, t) = 0, \quad t \geq 0, \quad i = \overline{1, k-1},$$

due to which inhomogeneous equation (39) takes the form

$$(\boldsymbol{w}_k)_t + (A(\boldsymbol{u})\boldsymbol{w}_k)_x = \boldsymbol{\Psi}[\boldsymbol{u}]. \quad (43)$$

The Cauchy problem for vector equation (43) with initial conditions (42), where $i = k$, generally has a non-zero solution $\boldsymbol{w}_k(x,t)$. Considering series (34), this gives up to $o(h^k)$ the leading disbalance term

$$\delta\boldsymbol{w}_h(x,t) = \boldsymbol{w}_h(x,t) - \boldsymbol{u}(x,t) = h^k\boldsymbol{w}_k(x,t) \tag{44}$$

for the solution $\boldsymbol{w}_h(x,t)$ of the PFDA (33), which makes it possible in the region $V_{\text{ex}}(x_*,t_*)$ to approximately estimate the error

$$\delta\boldsymbol{v}_h(x_j,t_n) = \boldsymbol{v}_h(x_j,t_n) - \boldsymbol{u}(x_j,t_n) = h^k\boldsymbol{w}_k(x_j,t_n) \tag{45}$$

of the numerical solution $\boldsymbol{v}_h(x_j,t_n)$ of the finite-difference Cauchy problem (20)–(23). Thus, in the simplest considered case, the convergence order (45) of the difference solution to the exact one coincides with the approximation order (30) by scheme (20) of system (5). This situation takes place in the region Λ_1 of the exact solution of problem (1), (2), when each of the considered schemes have the same orders of approximation (30) and convergence (45).

4.3. The accuracy of the numerical solution inside shock influence domain. Let us assume that the dependence set $V_{\text{ex}}(x_*,t_*)$ intersects with the shock of the exact solution $\boldsymbol{u}$ propagating in the positive direction of the x-axis and located on the line

$$L = \left\{(x,t):\ x = s(t),\ s'(t) > 0,\ t \geq t^* \geq 0\right\}, \tag{46}$$

where t^* is a time moment of shock formation. If $t^* = 0$, the shock arises as a result of the decay of a strong discontinuity in the initial data (6), and if $t^* > 0$, as a result of a gradient catastrophe inside the computational domain (further we will analyze in more detail the case $t^* = 0$). We will assume that the exact solution $\boldsymbol{u}$ of the problem (5), (6) is smooth in the domain $V_{\text{ex}}(x_*,t_*)\backslash L$ outside the shock L. Since the shock is a stable strong discontinuity [37], to which $m+1$ characteristics of system (5) come, and $m-1$ characteristics of this system go out from it, the shock L cannot immediately cross two lateral sides of the domain $V_{\text{ex}}(x_*,t_*)$, defined by formula (28). With this in mind, without loss of generality, we will assume that the shock L crosses the right boundary of the domain $V_{\text{ex}}(x_*,t_*)$, that is on the characteristic $x = L_1(t,x_*,t_*)$. For this case in Fig. 2 the dependence set $V_{\text{ex}}(x_*,t_*)$ is represented by a curvilinear triangle ABC.

Since in shock-capturing schemes there is no local convergence of the numerical solution to the exact one in some neighborhood of the shocks, we will assume that in considered domain $V_{\text{ex}}(x_*,t_*)\backslash L$, the semi-discrete numerical solution $\boldsymbol{w}_h(x,t_n)$ of the finite-difference Cauchy problem (31), (41) converges to the exact solution $\boldsymbol{u}(x,t)$ of the differential Cauchy problem (5), (6) in the sense of the following limit

$$\lim_{h\to 0} \|\ \boldsymbol{w}_h - \boldsymbol{u}\ \|_{V_{\varepsilon(h)}} = \lim_{h\to 0} \max_{(x,t_n)\in V_{\varepsilon(h)}} |\boldsymbol{w}_h(x,t_n) - \boldsymbol{u}(x,t_n)| = 0, \tag{47}$$

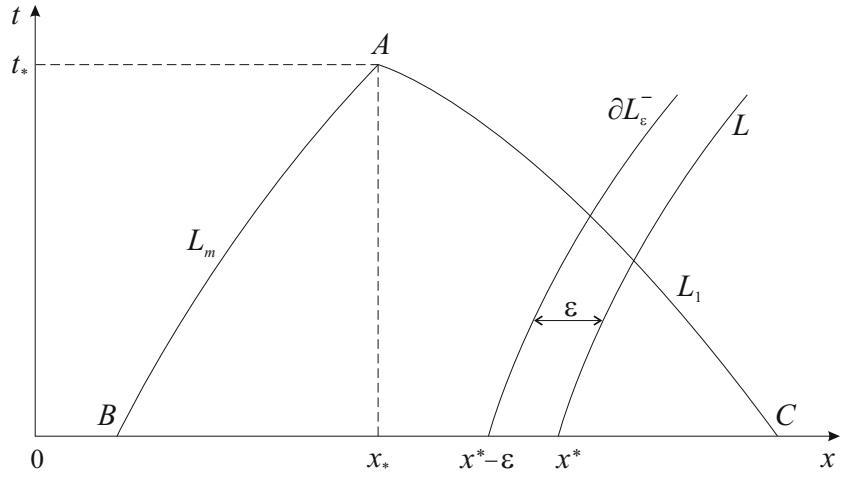

FIGURE 2. The dependence set of the exact solution at the point A that is inside the shock L influence domain.

where

$$\begin{gathered} V_\varepsilon = V_\varepsilon(x_*, t_*) = V_{\text{ex}}(x_*, t_*) \backslash L_\varepsilon, \\ L_\varepsilon = \{(x,t):\ s(t) - \varepsilon \le x \le s(t) + \varepsilon,\ t \ge 0\} \end{gathered} \tag{48}$$

is an ε-neighborhood of the shock L and $\varepsilon(h)$ is the positive monotonically decreasing function such that

$$\lim_{h\to 0} \varepsilon(h) = 0, \quad \lim_{h\to 0} h/\varepsilon(h) = 0. \tag{49}$$

It should be noted that the strong convergence assumption (47) for the NFC schemes is not always satisfied. It was shown [47] that when calculating the dam break problem for shallow water equations (1) with the parameter $z = 0.45$ in the stability condition (8), the numerical solutions obtained by the WENO5 [7] and CABARETM [48] schemes have undamped oscillations on some intervals inside the shock influence domain, where its amplitude does not decrease with decreasing numerical grid steps. As a result, taking into account the Lax-Wendroff theorem [36], the numerical solutions obtained by the NFC schemes WENO5 and CABARETM has only weak convergence to the constant exact solution inside the shock influence domain.

It follows from the passage to the limit (47) that at the left boundary

$$\partial L^-_{\varepsilon(h)} = \{(x,t) \in V_{\text{ex}}(x_*, t_*):\ x = s(t) - \varepsilon(h),\ t \ge 0\} \tag{50}$$

of the domain $L_{\varepsilon(h)}$ numerical solution $\boldsymbol{w}_h$ converges to the exact solution $\boldsymbol{u}$, i.e.

$$\lim_{h\to 0} \boldsymbol{w}_h(x, t_n) = \boldsymbol{u}(x, t_n), \quad (x, t_n) \in \partial L^-_{\varepsilon(h)}. \tag{51}$$

Assume first that this convergence is uniform and regular. This means that there is a natural number l and vector function $\boldsymbol{\psi}(x, t_n)$ for which up to $o(h^l)$

the condition

$$\boldsymbol{w}_h(x,t_n)=\boldsymbol{u}(x,t_n)+h^l\boldsymbol{\psi}(x,t_n),\quad (x,t_n)\in\partial L^-_{\varepsilon(h)},\tag{52}$$

is satisfied. Using a high-order interpolate function $\boldsymbol{\psi}(x,t_n)$ with respect to variable t, we extend the discrete-time condition (52) to the condition

$$\boldsymbol{w}_h(x,t)=\boldsymbol{u}(x,t)+h^l\boldsymbol{\psi}(x,t),\quad (x,t)\in\partial L^-_{\varepsilon(h)},\tag{53}$$

which depends on continuously changing variable t.

To construct the solutions $\boldsymbol{w}_i$ of systems (37)–(39) at the point (x_*,t_*) with initial conditions

$$\boldsymbol{w}_i(x,0)=0,\quad x\in I_{\varepsilon(h)}=\{x:\ (x,0)\in V_{\rm ex}(x_*,t_*),\ x\le s(0)-\varepsilon(h)\},\quad i=\overline{1,k},$$

it is necessary to set boundary conditions at the line $\partial L^-_{\varepsilon(h)}$. For this we substitute formula (53) in the expansion (34), written for $(x,t)\in\partial L^-_{\varepsilon(h)}$, and equate to zero the sums of coefficients for equal powers of h. As a result for $(x,t)\in\partial L^-_{\varepsilon(h)}$ we have

$$\boldsymbol{w}_i(x,t)=0,\quad i=\overline{1,k},\quad l>k,\tag{54}$$

$$\boldsymbol{w}_i(x,t)=0,\quad i=\overline{1,l-1},\quad \boldsymbol{w}_l(x,t)=\boldsymbol{\psi}(x,t),\quad l\le k.\tag{55}$$

In the general case, for the correctness of the initial-boundary value problems it is necessary that the number of scalar boundary conditions at the line $\partial L^-_{\varepsilon(h)}$ coincide with the number of characteristics of system (5) coming to the point (x_*,t_*) from this line. However, in our case, the boundary conditions (54) and (55) are correct, since they are not random, but are obtained from formula (53), which includes the exact $\boldsymbol{u}$ and approximated $\boldsymbol{w}_h$ solutions of the considered problem.

Taking into account the conditions (54) and (55), formally, three qualitatively different situations are possible when determining the main term of the numerical solution error at the point (x_*,t_*).

1. If $l>k$, the main error term is determined by the formula (44), where $\boldsymbol{w}_k(x,t)$ is the solution of the initial-boundary value problem for the system (43) with zero initial and boundary conditions

$$\boldsymbol{w}_k(x,0)=0,\ x\in I_{\varepsilon(h)};\quad \boldsymbol{w}_k(x,t)=0,\ (x,t)\in\partial L^-_{\varepsilon(h)}.$$

2. If $l=k$, the main error term is determined by the formula (44), where $\boldsymbol{w}_k(x,t)$ is the solution of the initial-boundary value problem for the system (43) with following initial and boundary conditions

$$\boldsymbol{w}_k(x,0)=0,\ x\in I_{\varepsilon(h)};\quad \boldsymbol{w}_k(x,t)=\boldsymbol{\psi}(x,t),\ (x,t)\in\partial L^-_{\varepsilon(h)}.$$

3. If $l<k$, the main error term is determined by the formula

$$\delta\boldsymbol{w}_h(x,t)=\boldsymbol{w}_h(x,t)-\boldsymbol{u}(x,t)=h^l\boldsymbol{w}_l(x,t),\tag{56}$$

where $\boldsymbol{w}_l(x,t)$ is the solution of the initial-boundary value problem for the homogeneous system

$$(\boldsymbol{w}_l)_t + (A(\boldsymbol{u})\boldsymbol{w}_l)_x = 0,$$

with the following initial and boundary conditions

$$\boldsymbol{w}_l(x,0) = 0,\ x \in I_{\varepsilon(h)}; \quad \boldsymbol{w}_l(x,t) = \boldsymbol{\psi}(x,t),\ (x,t) \in \partial L^-_{\varepsilon(h)}.$$

Thus, on the boundary condition (52), the main error term at the point (x_*, t_*) is given by regular formulas (44) or (56). We obtain a similar result on the condition $t^* > 0$ in formula (46), when the shock L arises as a result of a gradient catastrophe inside the computational domain. However, test calculations of the SPC problem (1), (2) by the NFC schemes showed [33] that in these schemes there is no regular convergence of the numerical solution to the exact one in the shock influence domains (4): the convergence orders (12) of the NFC schemes in these domains oscillate sharp around the value $r = 1$; the wavelength in these oscillations decreases in direct proportionality to decrease in grid step h and the amplitude of oscillations decreases much more slowly than the decrease in step h.

Taking this into account, for the NFC scheme, regulary boundary condition (52) is not satisfied, and the consequence of passage to the limit (51) is the more general formula

$$\boldsymbol{w}_h(x,t_n) = \boldsymbol{u}(x,t_n) + \boldsymbol{\psi}(h,x,t_n), \quad (x,t_n) \in \partial L^-_{\varepsilon(h)}, \tag{57}$$

where function $\boldsymbol{\psi}(h,x,t)$ satisfies the conditions

$$\lim_{h\to 0} |\boldsymbol{\psi}(h,x,t)| = 0, \quad \lim_{h\to 0} |\boldsymbol{\psi}(h,x,t)|/h = +\infty. \tag{58}$$

Moreover, function $\boldsymbol{\psi}(h,x,t)$ is not differentiable with respect to h, that makes it impossible to write condition (57) in regular form (52), which allows determining the local convergence order l. Here we will assume that function $\boldsymbol{\psi}(h,x,t)$ is sufficiently smooth with respect to its variables x and t.

Test calculations of the SPC problem also showed that the HASIA schemes, in contrast to the NFC schemes, retain the regular convergence of the numerical solution to the exact one inside shock influence domains (4). However, this convergence is not uniform: in particular [33], convergence orders of the RBM scheme inside shock influence domains is not constant, but is continuous function of independence variables x and t. This means that the numerical solution obtained by the HASIA scheme at the line (50) is given by formula (57), in which function $\boldsymbol{\psi}(h,x,t)$, for each value of $t = t_n$, can be represented in the form

$$\boldsymbol{\psi}(h,x,t) = h^{\alpha(t)}\bar{\boldsymbol{\psi}}(x,t) + o\left(h^{\alpha(t)}\right), \tag{59}$$

where $\bar{\boldsymbol{\psi}}(x,t)$ is some smooth function and $\alpha(t)$ is the positive continuous function determines the nonuniform convergence orders.

Using a high-order interpolate function $\boldsymbol{\psi}(h,x,t_n)$ with respect to variable t, we extend the discrete-time condition (57) to the condition

$$\boldsymbol{w}_h(x,t)=\boldsymbol{u}(x,t)+\boldsymbol{\psi}(h,x,t),\quad (x,t)\in\partial L^-_{\varepsilon(h)}, \tag{60}$$

which depends on the continuously changing variable t, where function $\boldsymbol{\psi}(h,x,t)$ satisfies conditions (58) for the NFC schemes and condition (59) for the HASIA schemes. To estimate the accuracy of the NFC scheme inside the shock influence domain, the PFDA-system (33) is applicable, which solution in this domain, in contrast to (34), should be found as follows

$$\boldsymbol{w}_h(x,t)=\boldsymbol{u}(x,t)+\boldsymbol{\omega}(h,x,t), \tag{61}$$

where with respect to function $\boldsymbol{\omega}(h,x,t)$, taking into account (58), we will assume that

$$O(|\boldsymbol{\omega}|)=O(|\boldsymbol{\psi}|)\ \Rightarrow\ \lim_{h\to0}|\boldsymbol{\omega}(h,x,t)|=0,\quad \lim_{h\to0}|\boldsymbol{\omega}(h,x,t)|/h=+\infty. \tag{62}$$

Substituting function (61) in the system (33), taking into account equation (5) and conditions (62), up to $o\,(|\boldsymbol{\omega}|)$ we obtain

$$\boldsymbol{\omega}_t+\left(A(\boldsymbol{u})\boldsymbol{\omega}\right)_x=0. \tag{63}$$

As a result, the main error term of the NFC scheme numerical solution inside shock influence domain is determined by the formula

$$\delta\boldsymbol{w}_h(x,t)=\boldsymbol{w}_h(x,t)-\boldsymbol{u}(x,t)=\boldsymbol{\omega}(h,x,t), \tag{64}$$

where $\boldsymbol{\omega}(h,x,t)$ is the solution of the initial-boundary value problem for the system (63) with following initial and boundary conditions

$$\begin{aligned}\boldsymbol{\omega}(h,x,0)=&0,\quad x\in I_{\varepsilon(h)};\\ \boldsymbol{\omega}(h,x,t)=&\boldsymbol{\psi}(h,x,t),\quad (x,t)\in\partial L^-_{\varepsilon(h)},\end{aligned} \tag{65}$$

where function $\boldsymbol{\psi}(h,x,t)$ satisfies the conditions (58).

To estimate the accuracy of the HASIA scheme inside shock influence domain, the solution of the PFDA-system (33) should be sought in the form (61), in which function $\boldsymbol{\omega}(h,x,t)$, considering (59), can be represented as follows

$$\boldsymbol{\omega}(h,x,t)=h^{\beta(x,t)}\overline{\boldsymbol{\omega}}(x,t)+o\left(h^{\beta(x,t)}\right), \tag{66}$$

where $\overline{\boldsymbol{\omega}}(x,t)$ is some smooth function and $\beta(x,t)$ is the positive continuous function determines the local convergence orders. Substituting such function (61) in the system (33), taking into account (5) and (66), up to $o\left(|\boldsymbol{\omega}|+h^k\right)$ we obtain

$$\boldsymbol{\omega}_t+\left(A(\boldsymbol{u})\boldsymbol{\omega}\right)_x=h^k\boldsymbol{\Psi}[\boldsymbol{u}]. \tag{67}$$

Thus the main error term of the HASIA scheme numerical solution inside shock influence domain is determined by the formula (64), where $\boldsymbol{\omega}(h,x,t)$ is the solution of initial-boundary value problem for the system (67) with the initial and boundary conditions (65), where function $\boldsymbol{\psi}(h,x,t)$ has the form (59).

4.4. The accuracy of the numerical solution inside centered rarefaction wave. Assume that the point (x_*, t_*) lies inside a centered rarefaction wave of index i

$$R = \left\{(x,t):\ L_i^-(t,x^*) \le x \le L_i^+(t,x^*),\quad t \ge 0\right\} \tag{68}$$

of the exact solution $\boldsymbol{u}$, where $x = L_i^{\mp}(t,x^*)$ are lateral characteristics of the i-th family coming from the point $P = (x^*, 0)$ on the x-axis and located at the left and right boundaries of the centered wave. At the center point $P = (x^*, 0)$ of the rarefaction wave (68) the initial function $\boldsymbol{u}_0(x)$ of the Cauchy problem (5), (6) is discontinuous

$$\boldsymbol{u}_0(x^* - 0) \ne \boldsymbol{u}_0(x^* + 0), \quad \lambda_i\left(\boldsymbol{u}_0(x^* - 0)\right) < \lambda_i(\boldsymbol{u}_0(x^* + 0)),$$

and at the lateral boundaries $x = L_i^{\mp}(t,x^*)$ of the wave (68), the exact solution $\boldsymbol{u}$ may have weak discontinuities, in particular, discontinuities of its first derivatives. We will assume that the exact solution $\boldsymbol{u}$ is smooth in dependence set $V_{\text{ex}}(x_*, t_*)$ outside boundary characteristics $x = L_i^{\mp}(t,x^*)$. In Fig. 3 the dependence set $V_{\text{ex}}(x_*, t_*)$ is represented by the curvilinear triangle ABC and the centered rarefaction wave R is located between characteristics L_i^- and L_i^+, emerging from the point $P = (x^*, 0)$.

Since in shock-capturing schemes there is no local convergence of the numerical solution to the exact one in some neighborhood of the center point P, we will assume that in the domain $V_{\text{ex}}(x_*, t_*)\backslash P$, the semi-discrete numerical solution $\boldsymbol{w}_h(x, t_n)$ of the finite-difference Cauchy problem (31), (41) converges to the exact solution $\boldsymbol{u}(x,t)$ of the differential Cauchy problem (5), (6) in the sense of the limit (47) where

$$\begin{aligned} V_\varepsilon =& V_\varepsilon(x_*, t_*) = V_{\text{ex}}(x_*, t_*)\backslash P_\varepsilon, \\ P_\varepsilon =& \left\{(x,t):\ (x - x^*)^2 + (t - t^*)^2 \le \varepsilon^2\right\} \end{aligned} \tag{69}$$

is an ε-neighborhood of the point P and $\varepsilon(h)$ is the positive monotonically decreasing function that satisfies the conditions (49). It follows from (47) that at part of the boundary

$$\begin{aligned} \partial P_{\varepsilon(h)} =& \\ =& \left\{(x,t) \in V_{\text{ex}}(x_*, t_*):\ (x - x^*)^2 + (t - t^*)^2 = \varepsilon^2(h),\ t \ge 0\right\} \end{aligned} \tag{70}$$

of the domain $P_{\varepsilon(h)}$ numerical solution $\boldsymbol{w}_h$ converges to the exact solution $\boldsymbol{u}$

$$\lim_{h \to 0} \boldsymbol{w}_h(x, t_n) = \boldsymbol{u}(x, t_n), \quad (x, t_n) \in \partial P_{\varepsilon(h)}.$$

It follows from the results of test calculations that inside the centered rarefaction waves, the shock-capturing schemes have the first convergence order, regardless of their approximation order (30). This means that at part

$$\begin{aligned} \partial P^*_{\varepsilon(h)} = \partial P_{\varepsilon(h)} \cap R =& \\ =& \left\{(x,t) \in R:\ (x - x^*)^2 + (t - t^*)^2 = \varepsilon^2(h)\right\} \end{aligned} \tag{71}$$

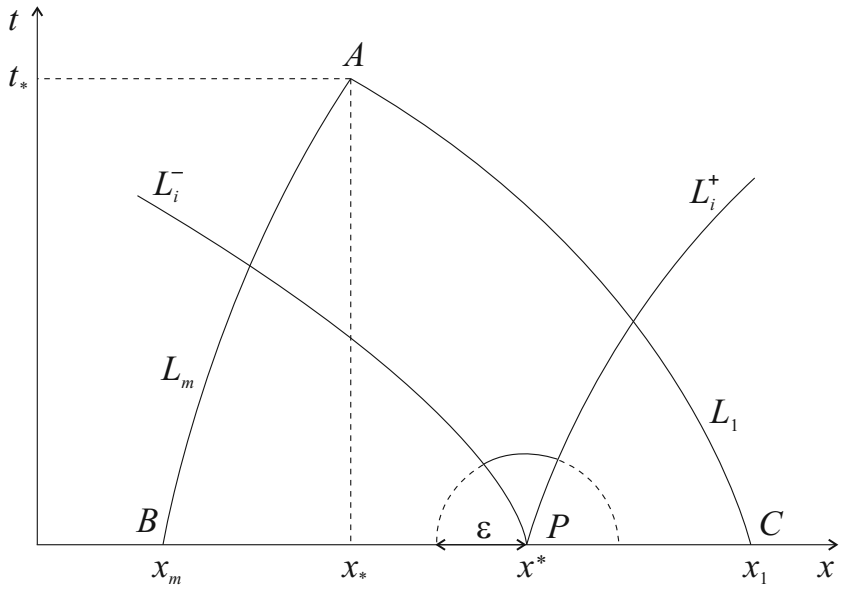

FIGURE 3. The dependence set of the exact solution at the point A that is inside the centered rarefaction wave.

of the boundary (70) located inside the centered wave (68), the numerical solution $\boldsymbol{w}_h(x,t_n)$ up to $o(h)$ can be represented as

$$\boldsymbol{w}_h(x,t_n)=\boldsymbol{u}(x,t_n)+h\boldsymbol{\psi}(x,t_n),\quad (x,t_n)\in\partial P^*_{\varepsilon(h)}, \tag{72}$$

where $\boldsymbol{\psi}(x,t_n)$ is some vector function. Using a high-order interpolate function $\boldsymbol{\psi}(x,t_n)$ along the line (71), we extend the discrete-time condition (72) to the condition

$$\boldsymbol{w}_h(x,t)=\boldsymbol{u}(x,t)+h\boldsymbol{\psi}(x,t),\quad (x,t)\in\partial P^*_{\varepsilon(h)}, \tag{73}$$

which depends on the continuously changing variable t.

Taking into account boundary condition (73), to obtain the error of the numerical solution inside centered rarefaction wave (68), we can use the PFDA-system (33), which solution is calculated in the form

$$\boldsymbol{w}_h(x,t)=\boldsymbol{u}(x,t)+h\boldsymbol{w}_1(x,t)+o(h). \tag{74}$$

Since we consider shock-capturing schemes of increased accuracy, for which the approximation order $k>1$, function $\boldsymbol{w}_1$ included in the expansion (74) satisfies homogeneous hyperbolic system (37) and zero initial conditions

$$\begin{gathered}\boldsymbol{w}_1(x,0)=0,\\ x\in I^*_{\varepsilon(h)}=\{x:\ (x,0)\in V_{\mathrm{ex}}(x_*,t_*),\ |x-x^*|\geq\varepsilon(h)\}.\end{gathered} \tag{75}$$

To set the boundary conditions that function $\boldsymbol{w}_1$ satisfies at the line (71), we substitute solution (74) in condition (73) and equating to zero the coefficients at h:

$$\boldsymbol{w}_1(x,t)=\boldsymbol{\psi}(x,t),\quad (x,t)\in\partial P^*_{\varepsilon(h)}. \tag{76}$$

In the general case, for the correctness of the initial-boundary value problems for the system (37) it is necessary that the number of scalar boundary conditions at the line $\partial P^*_{\varepsilon(h)}$ coincide with the number of characteristics of system (5) coming to the point $(x_*, t_*) \in R$ from this line. However, in our case, the vector boundary conditions (76) is correct, since they are not random, but is obtained from the formula (73), which includes the exact $\boldsymbol{u}$ and approximated $\boldsymbol{w}_h$ solutions of the considered problem. Thus the main term of the numerical solution error at the point $(x_*, t_*) \in R$ is determined by the formula

$$\delta \boldsymbol{w}_h(x,t) = \boldsymbol{w}_h(x,t) - \boldsymbol{u}(x,t) = h\boldsymbol{w}_1(x,t),$$

where $\boldsymbol{w}_1(x,t)$ is the solution of initial-boundary value problem for the system (37) with initial and boundary conditions (75) and (76) accordingly. Moreover, the convergence of the numerical solution $\boldsymbol{w}_h$ to the exact solution $\boldsymbol{u}$ inside the centered rarefaction wave (68) is uniform and regular.

4.5. Hyperbolic system of conservation laws admitting invariants. Let us multiply the hyperbolic system (5) on the left by matrix $L(\boldsymbol{u})$, which rows are the left eigenvectors of the Jacobian $A(\boldsymbol{u}) = \boldsymbol{f}_{\boldsymbol{u}}(\boldsymbol{u})$. Taking into account that

$$L(\boldsymbol{u})A(\boldsymbol{u}) = \Lambda(\boldsymbol{u})L(\boldsymbol{u}),$$

where $\Lambda(\boldsymbol{u})$ is a diagonal matrix of eigenvalues of the matrix $A(\boldsymbol{u})$, we obtain the characteristic representation of system (5)

$$L(\boldsymbol{u})\left(\boldsymbol{u}_t + \Lambda(\boldsymbol{u})\boldsymbol{u}_x\right) = 0. \tag{77}$$

Suppose that one of the differential form $l(\boldsymbol{u})d\boldsymbol{u}$, where $l(\boldsymbol{u})$ is some left eigenvector of the matrix $A(\boldsymbol{u})$, has an integrating factor $p(\boldsymbol{u})$, when multiplied by which it can be represented as a total differential

$$dF(\boldsymbol{u}) = p(\boldsymbol{u})l(\boldsymbol{u})d\boldsymbol{u} \tag{78}$$

of some function $F(\boldsymbol{u})$. In this case, the system (77) has an invariant

$$U = U(x,t) = F(\boldsymbol{u}(x,t)), \tag{79}$$

that satisfies equation

$$\left.\frac{dU}{dt}\right|_{\lambda(\boldsymbol{u})} = U_t + \lambda(\boldsymbol{u})U_x = 0, \tag{80}$$

where $\lambda(\boldsymbol{u})$ is the eigenvalue of the matrix $A(\boldsymbol{u})$ corresponding to its left eigenvector $l(\boldsymbol{u})$, i.e. $l(\boldsymbol{u})A(\boldsymbol{u}) = \lambda(\boldsymbol{u})l(\boldsymbol{u})$. Equation (80) implies that the invariant U remains constant on each characteristic $x = x_\lambda(t)$ given by the differential equation

$$\frac{dx}{dt} = \lambda(\boldsymbol{u}(x,t)).$$

Similarly, multiplying the PFDA-system (33) on the left by matrix $L(\boldsymbol{w}_h)$, we obtain the characteristic representation of this system

$$L(\boldsymbol{w}_h)\left((\boldsymbol{w}_h)_t + \Lambda(\boldsymbol{w}_h)(\boldsymbol{w}_h)_x\right) = h^k\boldsymbol{\Phi}[\boldsymbol{w}_h], \tag{81}$$

where $\mathbf{\Phi}[\boldsymbol{w}_h] = L(\boldsymbol{w}_h)\mathbf{\Psi}[\boldsymbol{w}_h]$. With formula (78) in mind, the system (81) has an invariant

$$W_h = W_h(x,t) = F(\boldsymbol{w}_h(x,t)), \tag{82}$$

that satisfies the inhomogeneous hyperbolic equation

$$\left.\frac{dW_h}{dt}\right|_{\lambda(\boldsymbol{w}_h)} = (W_h)_t + \lambda(\boldsymbol{w}_h)(W_h)_x = h^k \Phi[\boldsymbol{w}_h], \tag{83}$$

where $\Phi[\boldsymbol{w}_h] = p(\boldsymbol{w}_h)\phi[\boldsymbol{w}_h]$ and $\phi[\boldsymbol{w}_h]$ is corresponding component of the vector $\mathbf{\Phi}[\boldsymbol{w}_h]$. Let us study the accuracy with which invariant W_h of the numerical solution $\boldsymbol{w}_h$ approximates the invariant U of the exact solution $\boldsymbol{u}$ at some point (x_*, t_*), where $t_* > 0$.

4.5.1. The case when the exact solution is smooth in the dependence set $V_{\rm ex}(x_*, t_*)$. Assume that the exact solution $\boldsymbol{u}$ in the dependence set $V_{\rm ex}(x_*, t_*)$ is smooth. In this case, the main error term of the numerical solution $\boldsymbol{w}_h$ in the domain $V_{\rm ex}(x_*, t_*)$ is determined by the formula (44), so it follows that the numerical solution in this domain up to $o(h^k)$ can be represented as

$$\boldsymbol{w}_h(x,t) = \boldsymbol{u}(x,t) + h^k \boldsymbol{w}_k(x,t), \tag{84}$$

where function $\boldsymbol{w}_k(x,t)$ is the solution of the Cauchy problem for the system (43) with zero initial condition

$$\boldsymbol{w}_k(x,0) = 0, \quad x \in I = \{x : \ (x,0) \in V_{\rm ex}(x_*, t_*)\}.$$

Substituting expansion (84) in the formula (82), taking into account (79), we obtain

$$W_h(x,t) = F\left(\boldsymbol{u}(x,t) + h^k \boldsymbol{w}_k(x,t)\right) = \\ = U(x,t) + h^k F_{\boldsymbol{u}}(\boldsymbol{u}(x,t))\boldsymbol{w}_k(x,t) + o(h^k).$$

Hence it follows that numerical invariant W_h in the domain $V_{\rm ex}(x_*, t_*)$ up to $o(h^k)$ can be written as

$$W_h(x,t) = U(x,t) + h^k W_k(x,t), \tag{85}$$

where $W_k(x,t) = F_{\boldsymbol{u}}(\boldsymbol{u}(x,t))\boldsymbol{w}_k(x,t)$.

Substituting formulas (84) and (85) in the equation (83), we obtain

$$U_t + h^k (W_k)_t + \lambda\left(\boldsymbol{u} + h^k \boldsymbol{w}_k\right)\left(U_x + h^k (W_k)_x\right) = h^k \Phi[\boldsymbol{u} + h^k \boldsymbol{w}_k]. \tag{86}$$

Transforming the equation (86) using expansions

$$\lambda\left(\boldsymbol{u} + h^k \boldsymbol{w}_k\right) = \lambda(\boldsymbol{u}) + h^k \lambda_{\boldsymbol{u}}(\boldsymbol{u})\boldsymbol{w}_k + o(h^k), \quad \Phi[\boldsymbol{u} + h^k \boldsymbol{w}_k] = \Phi[\boldsymbol{u}] + O(h^k),$$

and considering equation (80), we equate to zero the sum of the coefficients at h^k. As a result, we have the hyperbolic equation

$$\left.\frac{dW_k}{dt}\right|_{\lambda(\boldsymbol{u})} = (W_k)_t + \lambda(\boldsymbol{u})(W_k)_x = \Phi[\boldsymbol{u}] - (\lambda_{\boldsymbol{u}}(\boldsymbol{u})\boldsymbol{w}_k)\, U_x \tag{87}$$

that function W_k satisfies with known functions $\boldsymbol{u}$, U and $\boldsymbol{w}_k$.

Since the sequence of equalities

$$W_h(x,0) = F(\boldsymbol{w}_h(x,0) = F(\boldsymbol{u}_0(x)) = F(\boldsymbol{u}(x,0)) = U(x,0)$$

follows from the initial conditions (6) and (41), taking into account formulas (79) and (82), the numerical invariant W_h satisfies the following initial condition

$$W_h(x,0) = U(x,0), \quad x \in I. \tag{88}$$

Substituting expansion (85) in the formula (88), we obtain

$$W_k(x,0) = 0, \quad x \in I, \tag{89}$$

Integrating equation (87) along the characteristic $x = x_\lambda(t, x_*, t_*)$ coming to the point (x_*, t_*) from some point $(x_*^0, 0)$, where $x_*^0 \in I$, with the initial condition (89) in mind, we have the formulas

$$W_k(x_*, t_*) = \int_0^{t_*} \Psi\left[\boldsymbol{V}\left(x_\lambda(t, x_*, t_*), t\right)\right] dt, \tag{90}$$

where we use the following notation

$$\boldsymbol{V} = (\boldsymbol{u}, \boldsymbol{w_k}, U), \quad \Psi[\boldsymbol{V}] = \Phi[\boldsymbol{u}] - (\lambda_{\boldsymbol{u}}(\boldsymbol{u})\boldsymbol{w}_k)\, U_x.$$

Thus, in the considered case, the calculation error of the invariant U at the point (x_*, t_*) up to $o(h^k)$ is determined by the formula

$$\delta W_h(x_*, t_*) = W_h(x_*, t_*) - U(x_*, t_*) = h^k W_k(x_*, t_*), \tag{91}$$

where the value $W_k(x_*, t_*)$ is given by (90). If system (77) admits one more invariant that extends along another family of characteristics $x = x_\mu(t)$, formulas (91) also take place for the calculation error of this invariant, taking into account the fact that in the integral in formula (90), characteristic $x_\lambda(t, x_*, t_*)$ should be replaced by characteristic $x_\mu(t, x_*, t_*)$. This means that all invariants of the system (77) are calculated at the point (x_*, t_*) with the same accuracy, which coincides with the accuracy of calculating the exact vector solution $\boldsymbol{u}$.

4.5.2. The case when the point (x_*, t_*) is inside the shock influence domain. Let us assume that the point (x_*, t_*) is inside the shock L influence domain (Fig. 2) and the exact solution $\boldsymbol{u}$ is smooth in the dependence set $V_{\text{ex}}(x_*, t_*) \backslash L$. Denote by $V^{\text{infl}}_{\varepsilon(h)}(x_*, t_*)$ that part of the domain $V_{\varepsilon(h)}(x_*, t_*)$, which intersects with the influence area of the shock L, where $V_\varepsilon(x_*, t_*)$ is given by formulas (48). In the considered case the NFC numerical solution $\boldsymbol{w}_h$ in the domain $W^{\text{infl}}_{\varepsilon(h)}(x_*, t_*)$ is representable in the form (61), and substituting it in the formula (82) with (79) in mind, we obtain

$$W_h(x,t) = F\left(\boldsymbol{u}(x,t) + \boldsymbol{\omega}(h,x,t)\right) = \\ = U(x,t) + F_{\boldsymbol{u}}(\boldsymbol{u}(x,t))\boldsymbol{\omega}(h,x,t) + o(|\boldsymbol{\omega}|).$$

Hence it follows that numerical invariant W_h in the domain $V^{\mathrm{infl}}_{\varepsilon(h)}(x_*, t_*)$ up to $o(|\boldsymbol{\omega}|)$ can be written as

$$W_h(x,t) = U(x,t) + \widetilde{W}(h,x,t), \tag{92}$$

where $\widetilde{W}(h,x,t) = F_{\boldsymbol{u}}(\boldsymbol{u}(x,t))\boldsymbol{\omega}(h,x,t)$. Substituting formulas (61) and (92) in the equation (83), taking into account equation (80) and conditions (62), up to $o\,(|\boldsymbol{\omega}|)$ we obtain the hyperbolic equation

$$\left.\frac{d\widetilde{W}}{dt}\right|_{\lambda(\boldsymbol{u})} = \widetilde{W}_t + \lambda(\boldsymbol{u})\widetilde{W}_x = -\left(\lambda_{\boldsymbol{u}}(\boldsymbol{u})\boldsymbol{\omega}\right) U_x \tag{93}$$

that function $\widetilde{W}$ satisfies with known functions $\boldsymbol{u}$, U and $\boldsymbol{\omega}$.

At first let us assume that characteristic $x = x_\lambda(t, x_*, t_*)$, coming at the point (x_*, t_*), goes out from the point $(x_\varepsilon, t_\varepsilon) \in \partial L^-_{\varepsilon(h)}$, i. e. from the point located at the left boundary (50) of the $\varepsilon(h)$-neighborhood of the shock L. Since at $(x,t) \in \partial L^-_{\varepsilon(h)}$ the sequence of equalities

$$\begin{aligned} W_h(x,t) = F(\boldsymbol{w}_h(x,t)) =& F(\boldsymbol{u}(x,t) + \boldsymbol{\psi}(h,x,t)) = \\ &= U(x,t) + F_{\boldsymbol{u}}(\boldsymbol{u}(x,t))\boldsymbol{\psi}(h,x,t) + o(|\boldsymbol{\psi}|) \end{aligned}$$

follows from the boundary condition (60), taking into account formulas (79) and (82), the function $\widetilde{W}$ in expansion (92) up to $o\,(|\boldsymbol{\psi}|)$ satisfies the boundary condition

$$\widetilde{W}(h,x,t) = \widetilde{\psi}(h,x,t) = F_{\boldsymbol{u}}(\boldsymbol{u}(x,t))\boldsymbol{\psi}(h,x,t), \quad (x,t) \in \partial L^-_{\varepsilon(h)}. \tag{94}$$

Integrating equation (93) along the characteristic $x = x_\lambda(t, x_*, t_*)$ on the time interval $[t_\varepsilon, t_*]$, with the boundary condition (94) in mind, we have the formula

$$\widetilde{W}(x_*, t_*) = \widetilde{\psi}(h, x_\varepsilon, t_\varepsilon) - \int_{t_\varepsilon}^{t_*} \widetilde{\Psi}\left[\widetilde{\boldsymbol{V}}\left(x_\lambda(t, x_*, t_*), t\right)\right] dt, \tag{95}$$

where we use the following notation

$$\widetilde{\boldsymbol{V}} = (\boldsymbol{u}, \boldsymbol{\omega}, U), \quad \widetilde{\Psi}[\widetilde{\boldsymbol{V}}] = \left(\lambda_{\boldsymbol{u}}(\boldsymbol{u})\boldsymbol{\omega}\right) U_x. \tag{96}$$

Formula (95) with conditions (58), (62) and formulas (94), (96), implies the estimate

$$\begin{aligned} \widetilde{W}(x_*, t_*) = O(|\boldsymbol{\psi}|) - (t_* - t_\varepsilon)O(|\boldsymbol{\omega}|)O(|U_x|) = \\ = O(|\boldsymbol{\psi}|)\,(1 - (t_* - t_\varepsilon)O(|U_x|) = O(|U_x|)O(|\boldsymbol{\psi}|). \end{aligned} \tag{97}$$

Suppose now that characteristic $x = x_\lambda(t, x_*, t_*)$, coming at the point (x_*, t_*), goes out from the point $(x^0_*, 0)$ on x-axis, where $x^0_* \in I_{\varepsilon(h)}$, and does not pass through the domain $L_{\varepsilon(h)}$. In this case, this characteristic at some point (x_b, t_b) crosses the boundary of the region $V^{\mathrm{infl}}_{\varepsilon(h)}(x_*, t_*)$, located inside the shock L influence domain. Since the exact solution $\boldsymbol{u}$ is smooth

in the dependence sets $V_{\mathrm{ex}}(x,t)$ of points (x,t) belonging to characteristic $x = x_\lambda(t, x_*, t_*)$ at $t \le t_b$, the numerical invariant W_h in this points up to $o(h^k)$ has the form (85). Substituting expansion (92) in formula (85) at $(x,t) = (x_b, t_b)$, we obtain an internal boundary condition

$$\begin{aligned} \widetilde{W}(h, x_b, t_b) &= h^k W_k(x_b, t_b), \\ W_k(x_b, t_b) &= F_{\boldsymbol{u}}(\boldsymbol{u}(x_b, t_b)\boldsymbol{w}_k(x_b, t_b), \end{aligned} \tag{98}$$

for the function $\widetilde{W}$ at the boundary of the shock influence domain. Integrating equation (93) along the characteristic $x = x_\lambda(t, x_*, t_*)$ on the time interval $[t_b, t_*]$, in respect of the notation (96) and boundary condition (98), we have

$$\widetilde{W}(x_*, t_*) = h^k W_k(x_b, t_b) - \int_{t_b}^{t_*} \widetilde{\Psi}\left[\widetilde{\boldsymbol{V}}\left(x_\lambda(t, x_*, t_*), t\right)\right] dt. \tag{99}$$

Because we conside shock-capturing schemes of high accuracy with approximation order $k \ge 2$, then formula (99) with conditions (62) and formulas (96), up to $o(|\boldsymbol{\psi}|)$ implies the estimate

$$\widetilde{W}(x_*, t_*) = (t_* - t_b)O(|\boldsymbol{\omega}|)O(|U_x|) = (t_* - t_b)O(|U_x|)O(|\boldsymbol{\psi}|). \tag{100}$$

Let us denote by U^s_ε the invariant transferred to the point (x_*, t_*) along the characteristic passing across the point $(x_\varepsilon, t_\varepsilon) \in \partial L^-_{\varepsilon(h)}$ and denote by U^s_b the invariant transferred to the point (x_*, t_*) along the characteristic passing across the point (x_b, t_b) that is at the boundary of the region $V^{\mathrm{infl}}_{\varepsilon(h)}(x_*, t_*)$. Comparison of formulas (97) and (100) shows that, if the inequality

$$(t_* - t_b)\,|(U^s_b)_x| \ll |(U^s_\varepsilon)_x|$$

is satisfied in the region $V^{\mathrm{infl}}_{\varepsilon(h)}(x_*, t_*)$, then the invariant U^s_ε is calculated at the point (x_*, t_*) with a significantly lower accuracy than the invariant U^s_b. We can obtain a similar result for the HASIA schemes, provided that the local convergence orders in formulas (59) and (66) satisfy inequalities

$$\alpha(t) \ll k, \quad \beta(x,t) \ll k,$$

where k is the order of approximation of the scheme. We note that above situation takes place [27, 28, 30, 32, 33] in the numerical solution of the SPC problem (1), (2) according to high order shock-capturing schemes, when in the shock influence domains (4), invariant w_1, transferred to these domains through the shocks, is calculated with a significantly lower accuracy than the invariant w_2, transferred to these domains from x-axis through the smoothness region of the exact solution.

4.5.3. The case when the point (x_*, t_*) is inside the centered rarefaction wave. Suppose that the point (x_*, t_*) is inside the centered rarefaction wave (68) of the exact solution $\boldsymbol{u}$ and this solution is smooth in the dependence set $V_{\mathrm{ex}}(x_*, t_*)$ outside boundary characteristics $x = L^{\mp}_i(t, x^*)$

of the rarefaction wave. Denote by $V^{\rm rar}_{\varepsilon(h)}(x_*,t_*)$ that part of the domain $V_{\varepsilon(h)}(x_*,t_*)$, which intersects with the rarefaction wave (68), where $V_\varepsilon(x_*,t_*)$ is given by formulas (69). In the considered case the numerical solution $\boldsymbol{w}_h$ in the domain $V^{\rm rar}_{\varepsilon(h)}(x_*,t_*)$ is representable in the form (74), substituting which in the formula (82) with (79) in mind, we obtain

$$W_h(x,t) = F\left(\boldsymbol{u}(x,t) + h\boldsymbol{w}_1(x,t) + o(h)\right) = \\ = U(x,t) + hF_{\boldsymbol{u}}(\boldsymbol{u}(x,t))\boldsymbol{w}_1(x,t) + o(h).$$

Hence it follows that numerical invariant W_h in the domain $S^{\rm rar}_{\varepsilon(h)}(x_*,t_*)$ up to $o(h)$ can be written as

$$W_h(x,t) = U(x,t) + hW_1(x,t), \tag{101}$$

where $W_1(x,t) = F_{\boldsymbol{u}}(\boldsymbol{u}(x,t))\boldsymbol{w}_1(x,t)$. Substituting formulas (74) and (101) in equation (83), taking into account equation (80) and inequality $k \geq 2$, up to $o(h)$ we obtain the hyperbolic equation

$$\left.\frac{dW_1}{dt}\right|_{\lambda(\boldsymbol{u})} = (W_1)_t + \lambda(\boldsymbol{u})(W_1)_x = -\left(\lambda_{\boldsymbol{u}}(\boldsymbol{u})\boldsymbol{w}_1\right)U_x \tag{102}$$

that function W_1 satisfies with known functions $\boldsymbol{u}$, U and $\boldsymbol{w}_1$.

At first let us assume that characteristic $x = x_\lambda(t,x_*,t_*)$, coming at the point (x_*,t_*), is a characteristic of i-th family coming from the center point $P = (x^*,0)$ of the rarefaction wave (68) and intersecting at the point $(x_\varepsilon,t_\varepsilon)$ boundary line $\partial P^*_{\varepsilon(h)}$ of $\varepsilon(h)$-neighborhood of the center point P. Since at $(x,t) \in \partial P^*_{\varepsilon(h)}$ the sequence of equalities

$$W_h(x,t) = F(\boldsymbol{w}_h(x,t)) = F(\boldsymbol{u}(x,t) + h\boldsymbol{\psi}(x,t)) = \\ = U(x,t) + hF_{\boldsymbol{u}}(\boldsymbol{u}(x,t))\boldsymbol{\psi}(x,t) + o(h)$$

follows from the boundary condition (73), taking into account formulas (79) and (82), the function W_1 in expansion (101) up to $o(h)$ satisfies the boundary condition

$$W_1(x,t) = \overline{\psi}(x,t) = F_{\boldsymbol{u}}(\boldsymbol{u}(x,t))\boldsymbol{\psi}(x,t), \quad (x,t) \in \partial P^*_{\varepsilon(h)}. \tag{103}$$

Integrating equation (102) along the characteristic $x = x_\lambda(t,x_*,t_*)$ on the time interval $[t_\varepsilon,t_*]$, with the boundary condition (103) in mind, we have the formula

$$W_1(x_*,t_*) = \overline{\psi}(x_\varepsilon,t_\varepsilon) - \int\limits_{t_\varepsilon}^{t_*} \overline{\Psi}\left[\overline{\boldsymbol{V}}\left(x_\lambda(t,x_*,t_*),t\right)\right]dt, \tag{104}$$

where we use the following notation

$$\overline{\boldsymbol{V}} = (\boldsymbol{u},\boldsymbol{w}_1,U), \quad \overline{\Psi}\left[\overline{\boldsymbol{V}}\right] = \left(\lambda_{\boldsymbol{u}}(\boldsymbol{u})\boldsymbol{w}_1\right)U_x. \tag{105}$$

Formula (104), with (101) and (105), implies the estimate for numerical invariant error

$$\delta W_h(x_*,t_*) = W_h(x_*,t_*) - U(x_*,t_*) = hW_1(x_*,t_*) = \\ = O(h)\,(1-(t_*-t_\varepsilon)O(|U_x|)) = O(|U_x|)O(h). \quad (106)$$

Suppose now that characteristic $x = x_\lambda(t,x_*,t_*)$, coming at the point (x_*,t_*), goes out from the point $(x_*^0,0)$ on x-axis, where $x_*^0 \in I^*_{\varepsilon(h)}$, and does not pass through the domain $P_{\varepsilon(h)}$. In this case, the characteristic at some point (x_b,t_b) crosses the boundary of the region $V^{\mathrm{rar}}_{\varepsilon(h)}(x_*,t_*)$. Since the exact solution $\boldsymbol{u}$ is smooth in the dependence sets $V_{\mathrm{ex}}(x,t)$ of points (x,t) belonging to characteristic $x = x_\lambda(t,x_*,t_*)$ at $t \le t_b$, the numerical invariant W_h in this points up to $o(h^k)$ has the form (85). Substituting expansion (101) in the formula (85) at $(x,t) = (x_b,t_b)$ and considering that $k \ge 2$, we obtain an internal boundary condition

$$W_1(x_b,t_b) = 0 \quad (107)$$

at the boundary of the centered rarefaction wave. Integrating equation (102) along the characteristic $x = x_\lambda(t,x_*,t_*)$ on the time interval $[t_b,t_*]$, taking into account the notation (105) and boundary condition (107), we have

$$W_1(x_*,t_*) = -\int_{t_b}^{t_*} \overline{\Psi}\left[\overline{\boldsymbol{V}}\left(x_\lambda(t,x_*,t_*),t\right)\right] dt. \quad (108)$$

Formula (108), with (101) and (105), implies the estimate for numerical invariant error

$$\delta W_h(x_*,t_*) = W_h(x_*,t_*) - U(x_*,t_*) = hW_1(x_*,t_*) = \\ = (t_*-t_b)O(|U_x|)O(h). \quad (109)$$

Let us denote by U^r_ε the invariant transferred to the point (x_*,t_*) along the characteristic passing across the point $(x_\varepsilon,t_\varepsilon) \in \partial P^*_{\varepsilon(h)}$ and denote by U^r_b the invariant transferred to the point (x_*,t_*) along the characteristic passing across the point (x_b,t_b) that is at the boundary of the region $V^{\mathrm{rar}}_{\varepsilon(h)}(x_*,t_*)$. Comparison of formulas (106) and (109) shows that, if the inequality

$$(t_*-t_b)\,|(U^r_b)_x| \ll |(U^r_\varepsilon)_x| \quad (110)$$

is satisfied in the region $V^{\mathrm{rar}}_{\varepsilon(h)}(x_*,t_*)$, then the invariant U^r_ε is calculated at the point (x_*,t_*) with a significantly lower accuracy than the invariant U^r_b.

Thus, we have given a theoretical justification for the fact that in the shock influence domains and inside the centered rarefaction waves, different invariants of the approximated hyperbolic system can be calculated with significantly different accuracy.

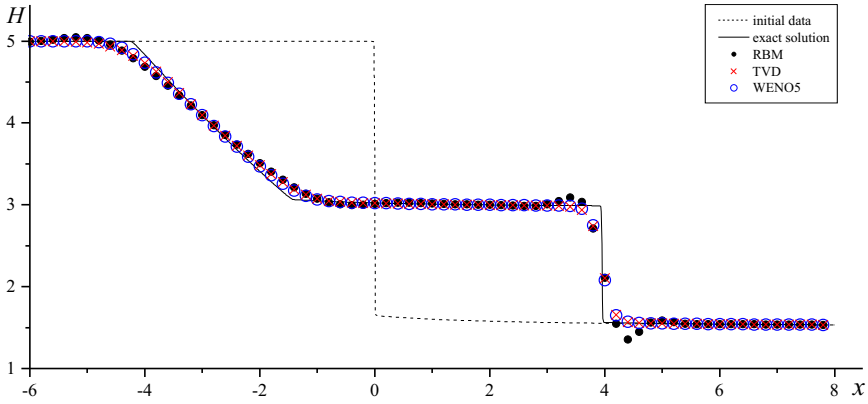

FIGURE 4. Liquid depth obtained by solving the modified dam break problem (1), (111) at time $t = 0.6$. Initial data (*dashed line*) and exact solution (*solid line*) that simulated by numerical calculation with the step $h = 0.001$ by the WENO5. Numerical calculations with the step $h = 0.2$ by the schemes: RBM (*points*), TVD (*crosses*) and WENO5 (*circles*).

5 Modified dam break problem

To illustrate the theoretical results obtained in the previous section, we will use test calculations by the RBM, TVD and WENO5 finite-difference schemes of the Cauchy problem for shallow water equations (1) with the following piecewise smooth discontinuous initial data

$$H(x,0) = \begin{cases} H_1, & x \le 0, \\ \varphi(x), & x > 0, \end{cases} \qquad q(x,0) = 0, \tag{111}$$

where $H_1 = 5$,

$$\varphi(x) = 2 - \frac{1}{\pi}\arctan(x+2). \tag{112}$$

From formulas (111) and (112) it follows that the initial depth function $H(x,0)$ at $x = 0$ has a strong discontinuity

$$H(0,0) - H(0+0,0) = 3 + \frac{1}{\pi}\arctan(2) \approx 3.35. \tag{113}$$

Since Cauchy problem (1), (111) differs from the classical dam break problem only that in the initial data (111) the liquid depth in the lower pool of the dam is not constant, but monotonically decreasing function (112), we will designate the problem (1), (111) as Modified Dam Break (MDB) problem.

In the exact solution of the MDB problem (solid line in Fig. 4), as a result of the decay of the initial discontinuity (113), it is formed L shock (46) of index $i = 2$ and R centered rarefaction waves (68) of index $i = 1$ with $x^* = 0$, between which a smooth flow region V_{LR} is located, where the liquid level decreases monotonically. Before the shock L, by the evolution of the

initial liquid depth given by formula (112), another smooth flow region V_L is formed, where the liquid level also decreases monotonically. On the left of the rarefaction wave R there is region V_R, where the liquid is at rest and has the initial depth H_1. Thus, in the considered problem we have four qualitatively different regions of smoothness for the exact solution, namely: R, V_{LR}, V_L and V_R. Moreover, the region V_R, where the exact solution is constant, is special, since all the schemes reproduce this constant solution accurately, due to which the errors of numerical solutions in this region are equal to zero, and the local convergence orders are not defined.

Figs. 4–6 present the results of the MDB problem calculations at time $t = 0.6$ by the RBM, TVD and WENO5 schemes on the numerical grid (7), where $\tau/h = 0.05$, which guarantees the fulfillment of the stability condition (8). Fig. 4 shows a comparison of the exact solution for the liquid depth with the results of calculations on the numerical grid (7) with the spatial step $h = 0.2$. The exact solution is simulated with numerical calculation by the WENO5 on a fairly fine grid (7) with a spatial step $h = 0.001$. We can see from Fig. 4 that the HASIA scheme RBM has noticeable oscillations at the shock, which are absented in the NFC schemes TVD and WENO5. Fig. 5 represent the averaged local convergence orders (18) of numerical solutions to the exact vector solution $\boldsymbol{u} = (H, q)$, as well as to its invariants $w_1 = u - 2c$ and $w_2 = u + 2c$. Note that in some neighborhoods of the shock L and weak discontinuities at the boundary of the wave R, where the exact solution is not smooth, the local convergence orders are not defined and therefore their formal values, obtained from formulas (18), give typical fluctuations in these neighborhoods that have no connection to real convergence orders (the indicated neighborhood of the left boundary of the wave R in Figs. 5 and 6 are not shown). Fig. 6 show relative errors (19) in calculating the vector solution $\boldsymbol{u}$ and its invariants w_1 and w_2. Calculations of the convergence orders and relative errors are performed on the basic grid (7) with the spatial step $h = 0.02$ and are shown for each 15th spatial node $j = 15i$ of the basic grid.

Since for each point $(x_*, t_*) \in V_L$ the dependence set $V_{\text{ex}}(x_*, t_*) \subset V_L$, where V_L is the smoothness region of the exact solution $\boldsymbol{u}$, located in front of the shock L (at $x > 4$ in Figs. 4–6), in accordance with theoretical Sections 4.2 and 4.5.1, the convergence orders (18) of all three considered schemes in the region V_L coincide with their approximation orders (30); for the RBM and WENO5 schemes it is the third order, and for the TVD scheme it is the second order (Fig. 5). From here, in particular, it follows that, in the region V_L for all these schemes, the convergence orders $\bar{r}$ to the vector solution $\boldsymbol{u}$ coincide with the scalar convergence orders $\bar{\rho}_1$ and $\bar{\rho}_2$ to the invariants w_1 and w_2. Despite this, the accuracy of calculation of the invariants w_1 and w_2 in the region V_L is different (Fig. 6), namely, for all schemes invariant w_1 is calculated with significantly higher accuracy than invariant w_2. This is explained by the fact that invariant w_1 is transferred

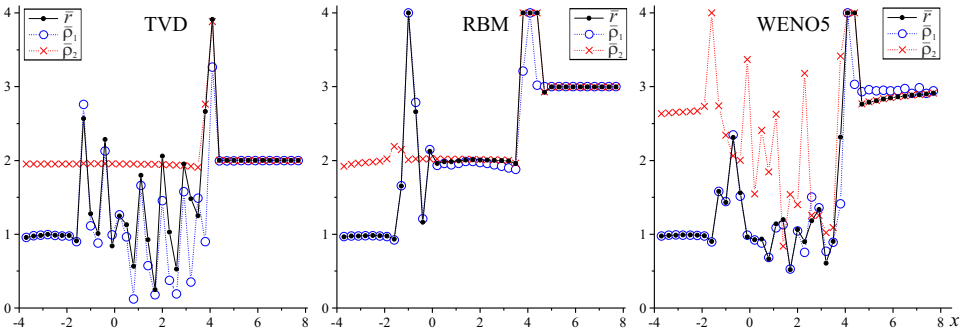

FIGURE 5. The averaged local convergence orders (18) to the exact vector solution $\boldsymbol{u}$ (*points*) and to its invariants w_1 (*circles*), w_2 (*crosses*), obtained by the TVD, RBM and WENO5 schemes.

to the point $(x_*, t_*) \in V_L$ along the characteristic $x = L_1(t, x_*, t_*)$ propagating with the velocity $\lambda_1 = u - c < 0$ from the region $x > x_*$, where the flow is smoother and absolute values of the derivatives of the exact solution are significantly smaller than in the region $s(t) < x < x_*$, from where the invariant w_2 is transferred to the point (x_*, t_*) along the characteristic $x = L_2(t, x_*, t_*)$ propagating with the velocity $\lambda_2 = u + c > 0$. As a result, the absolute value of the integral in the right side of the formula (90) for the numerical solution error in the case of the invariant w_1 is significantly less than in the case of the invariant w_2. From Fig. 6 it also follows that in the region V_L the accuracy of the TVD scheme, which has the second order of approximation, is noticeably lower than that of the RBM and WENO5 schemes, which have the third order of approximation. At the same time, the accuracy of the WENO5 scheme in the region V_L is significantly higher than for the RBM scheme, since the WENO5 scheme has the fifth order of spatial approximation, while the RBM scheme has only the third order of spatial approximation.

From Fig. 5 it follows that (in accordance with the results of theoretical Sections 4.4 and 4.5.3) inside the centered rarefaction wave R located in Fig. 4 on the interval $(-4.4, -1.5)$ outside some vicinity of R wave boundaries $x = L_1^{\mp}(t)$ all considered schemes have the first order of vector convergence which coincides with the scalar convergence order ($\bar{r} = \bar{\rho}_1 = 1$) to invariant w_1, transferred to the region R along characteristics $x = L_1(t)$ emerging from the wave center $P = (0, 0)$, located at the point of discontinuity of the initial data (111). With this in mind, inside the wave R (Fig. 6) all the schemes in calculations of the vector solution $\boldsymbol{u}$ have almost identical errors $\Delta \boldsymbol{v}_h$, given by the first formula (19), which are very close to the errors $\Delta(w_1)_h$ that are given by the second formula (19) and are obtained when calculating the invariant w_1. Moreover, for all considered schemes, the accuracy of calculation of the invariant w_2 in the wave R is several orders of magnitude higher than for the invariant w_1 and vector solution $\boldsymbol{u}$, which leads (Fig. 5)

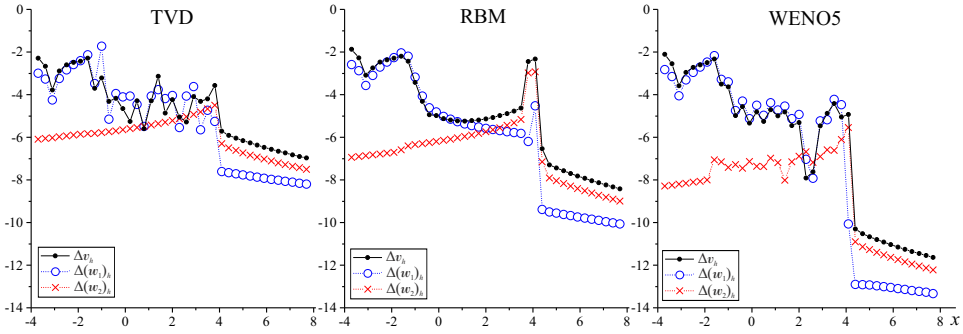

FIGURE 6. The relative errors (19) in calculating vector solution $\boldsymbol{u}$ (*points*) and its invariants w_1 (*circles*), w_2 (*crosses*), obtained by the TVD, RBM and WENO5 schemes.

to higher orders of convergence to invariant w_2 inside the wave R: $\bar{\rho}_2 = 2$ for the RBM and TVD schemes, $\bar{\rho}_2 = 2.6$ for the WENO5 scheme. This is explained by the fact that the exact solution inside the centered R wave is close to the exact solution inside the self-similar centered rarefaction wave (obtained by solving the classical dam break problem), where the invariant $w_2 = \text{const}$. Therefore, inside the wave R the inequality

$$|(w_2)_x| \ll |(w_1)_x|$$

is satisfied, which, taking into account formulas (106), (109) and inequality (110), leads to the above-mentioned difference in the accuracy of calculation of the invariants w_1 and w_2.

The smooth flow region V_{LR} located in Fig. 4 on the interval $(-1.5, 4)$ between the shock L and the centered wave R is the L shock influence domain, since the characteristics of the first family $x = L_1(t)$ passing through the L shock come into V_{LR}. At the same time, the region V_{LR} is the R wave influence domain, since it gets the characteristics of the second family $x = L_2(t)$ passing through the wave R. Fig. 5 shows that on the interval $(0, 3.5)$ inside the region V_{LR} the RBM scheme provides the second-order convergence ($\bar{r} = \bar{\rho}_1 = \bar{\rho}_2 = 2$) both to the vector solution $\boldsymbol{u}$ and to its invariants w_1 and w_2. This means that, in contrast to the SPC problem given in the introduction, which solution obtained by the RBM scheme leads [33] to non-uniform regular convergence (61), (66) inside the shock influence domains, when solving the MDB problem, the RBM scheme provides uniform regular convergence with the second order

$$\boldsymbol{w}_h(x,t) = \boldsymbol{u}(x,t) + h^2 \boldsymbol{w}_2(x,t) + o(h) \tag{114}$$

inside the region V_{LR}. Function $\boldsymbol{w}_2(x,t)$, which determines in the expansion (114) the main error term of the numerical solution $\boldsymbol{v}_h$, is obtained by solving inside the region V_{LR} for the homogeneous vector equation

$$(\boldsymbol{w}_2)_t + (A(\boldsymbol{u})\boldsymbol{w}_2)_x = 0,$$

a boundary value problem with boundary conditions at some lines located in the region V_{LR} near its lateral boundaries, where the numerical solution $\boldsymbol{v}_h$ converges to the exact solution $\boldsymbol{u}$ with the second order. As a result, inside the region V_{LR}, the RBM scheme has a fairly close accuracy (Fig. 6) in calculations of the vector solution $\boldsymbol{u}$ and its invariants w_1 and w_2.

From Fig. 5 it follows that inside the region V_{LR}, the formal convergence orders $\bar{r}$ and $\bar{\rho}_1$ of numerical solutions obtained according to the formulas (18) by the TVD and WENO5 schemes oscillate sharp around the value $r = 1$. Taking into account the results of Section 4.3, this means that the TVD and WENO5 schemes inside the region V_{LR} do not provide regular local convergence to the exact vector solution $\boldsymbol{u}$ and its invariant w_1, which is due to the irregularity of the boundary condition (57) generated by the numerical solution at the line $\partial L^{-}_{\varepsilon(h)}$. Moreover (Fig. 6), in the WENO5 scheme the accuracy of calculation of the invariant w_2 in the region V_{LR} is several orders of magnitude higher than for the invariant w_1 and vector solution $\boldsymbol{u}$, which (in accordance with Section 4.5.2) is associated with the higher approximation accuracy of the invariant w_2 in the neighborhood of the left boundary of the region V_{LR}. Fig. 5 also shows that in the region V_{LR} for the NFC schemes TVD and WENO5, the convergence orders $\bar{\rho}_2$ to invariant w_2 are significantly higher than convergence orders $\bar{r}$ and $\bar{\rho}_1$ to the exact solution $\boldsymbol{u}$ and invariant w_1. In the numerical solution obtained by the WENO5 scheme, the convergence orders $\bar{\rho}_2$ in the region V_{LR} oscillate noticeably, that indicates the absence of regular convergence to the invariant w_2 in this region. At the same time, in the numerical solution obtained by the TVD scheme, in the region V_{LR} (as well as inside the wave R), the convergence order $\bar{\rho}_2 = 2$, which means uniform regular convergence to the invariant w_2 in this region. As a result, the errors $\Delta(w_2)_h$ in calculation of the invariant w_2 in the region V_{LR} for the TVD scheme strictly monotonically increase, and for the WENO5 scheme they oscillate noticeably (Fig. 6).

6 Conclusion

The test calculations of the MDB problem (1), (111) by the high order shock-capturing RBM, TVD and WENO5 finite-difference schemes showed (Fig. 4–6) that the maximum loss of the accuracy in these schemes occurs inside the centered rarefaction R wave. Within the wave R , all three considered schemes have (Fig. 5) the first convergence order to the exact vector solution $\boldsymbol{u}$, which is associated with the first convergence order to the invariant $w_1 = u - 2c$ of this solution, transferred along the characteristics emanating from the center of the wave R (the convergence order to the invariant $w_2 = u + 2c$ inside the wave R is significantly higher). As a result (Fig. 6), for these schemes inside the wave R the accuracy of calculation of the vector solution $\boldsymbol{u}$ and its invariant w_1 is approximately the same, while invariant w_2 is calculated with significantly higher accuracy. In this case, the HASIA scheme RBM, in contrast to the NFC schemes TVD and

WENO5, retains the second convergence order in the main part of the shock L influence domain (Fig. 5), which is also the R wave influence domain. This means that the combined shock-capturing schemes constructed in [33], where the RBM scheme is used as a basic one, and the NFC schemes CU [10] or A-WENO [49] are used as internal schemes, when calculating the MDB problem will monotonically localize the shock L and simultaneously keep an increased accuracy in the shock influence domain V_{LR}. At the same time, these combined schemes will have only the first convergence order inside the centered rarefaction wave R, coinciding with the convergence order of the basic RBM scheme. Thus, for the further successful development of the theory and applications of shock-capturing combined schemes [32, 33], first of all it is necessary to solve the problem of maintaining the increased accuracy of the basic HASIA schemes inside centered rarefaction waves. If these centered waves arise when solving the Cauchy problem with the discontinuous initial data, then in order to achieve the required accuracy of the HASIA scheme, calculation should be carried out on a significantly finer numerical grid (compared to the basic grid) on some initial time interval.

References

[1] S.K. Godunov, *A difference method for numerical calculation of discontinuous solutions of the equations of hydrodynamics*, Mat. Sb., **47**:3 (1959), 271–306. Zbl 0171.46204

[2] B. van Leer, *Toward the ultimate conservative difference scheme. V. A second-order sequel to Godunov's method*, J. Comput. Phys., **32**:1 (1979), 101–136. Zbl 1364.65223

[3] A. Harten, *High resolution schemes for hyperbolic conservation laws*, J. Comput. Phys., **49** (1983), 357–393. Zbl 0565.65050

[4] A. Harten, S. Osher, *Uniformly high-order accurate nonoscillatory schemes*, SIAM J. Numer. Analys., **24**:2 (1987) 279–309. Zbl 0627.65102

[5] H. Nessyahu, E. Tadmor, *Non-oscillatory central differencing for hyperbolic conservation laws*, J. Comput. Phys., **87**:2 (1990), 408–463. Zbl 0697.65068

[6] X.-D. Liu, S. Osher, T. Chan, *Weighted essentially non-oscillatory schemes*, J. Comput. Phys., **115**:1 (1994), 200–212. Zbl 0811.65076

[7] G.S. Jiang, C.W. Shu, *Efficient implementation of weighted ENO schemes*, J. Comput. Phys. **126** (1996), 202–228. Zbl 0877.65065

[8] B. Cockburn, *An introduction to the discontinuous Galerkin method for convection-dominated problems*, Lect. Notes Math. **1697** (1998), 150–268. Zbl 0927.65120

[9] A. Kurganov, E. Tadmor, *New high-resolution central schemes for nonlinear conservation laws and convection-diffusion equations*, J. Comput. Phys., **160**:1 (2000), 241–282. Zbl 0987.65085

[10] A. Kurganov, S. Noelle, G. Petrova, *Semidiscrete central-upwind schemes for hyperbolic conservation laws and Hamilton-Jacobi equations*, SIAM J. Sci. Comput. **23**:3 (2001), 707–740. Zbl 0998.65091

[11] S.A. Karabasov, V.M. Goloviznin, *Compact accurately boundary-adjusting high-resolution technique for fluid dynamics*, J. Comput. Phys., **228**:19 (2009), 7426–7451. Zbl 1172.76034

[12] A. Gelb, E. Tadmor, *Adaptive edge detectors for piecewise smooth data based on the minmod limiter*, J. Sci. Comput., **28** (2006), 279–306.

[13] F. Arandiga, A. Baeza, R. Donat, *Vector cell-average multiresolution based on Hermite interpolation*, Adv. Comput. Math. **28**:1 (2008), 1–22. Zbl 1131.65007
[14] J.L. Guermond, R. Pasquetti, B. Popov, *Entropy viscosity method for nonlinear conservation laws*, J. Comput. Phys., **230** (2011), 4248–4267.
[15] J. Dewar, A. Kurganov, M. Leopold, *Pressure-based adaption indicator for compressible Euler equations*, Numer. Methods Partial Differ. Equ., **31** (2015), 1844–1874.
[16] R.J. LeVeque, *Finite volume methods for hyperbolic problems*, Cambridge: Cambridge University Press, 2002.
[17] E.F. Toro, *Riemann solvers and numerical methods for fluid dynamics: practical introduction*, Berlin: Springer-Verlag, 2009.
[18] J.S. Hesthaven, *Numerical methods for conservation laws*, Society for Industrial and Applied Mathematics (SIAM), Philadelphia, PA, 2018.
[19] C.W. Shu, *Essentially non-oscillatory and weighted essentially non-oscillatory schemes*, Acta Numerica, **29** (2020), 701–762.
[20] V.V. Ostapenko, *Convergence of difference schemes behind a shock front*, Comput. Math. Math. Phys., **37**:10 (1997), 1161–1172. Zbl 1122.76355
[21] J. Casper, M.H. Carpenter, *Computational considerations for the simulation of shock-induced sound*, SIAM J. Sci. Comput., **19**:3 (1998), 813–828.
[22] B. Engquist, B. Sjogreen, *The convergence rate of finite difference schemes in the presence of shocks*, SIAM J. Numer. Anal., **35**:6 (1998), 2464–2485..
[23] O.A. Kovyrkina, V.V. Ostapenko, *On the practical accuracy of shock-capturing schemes*, Math. Models Comput. Simul., **6**:2 (2014), 183–191.
[24] J.J. Stoker, *Water Waves: The Mathematical Theory with Applications*, Wiley-Interscience, 1957.
[25] N.A. Mikhailov, *The convergence order of WENO schemes behind a shock front*, Math. Models. Comput. Simul. **7**:5 (2015), 467–474.
[26] M.E. Ladonkina, O.A. Neklyudova, V.V. Ostapenko, V.F. Tishkin, *On the accuracy of the discontinuous Galerkin method in calculation of shock waves*, Comput. Math. Math. Phys., **58**:8 (2018), 1344–1353.
[27] O.A. Kovyrkina, V.V. Ostapenko, *On the construction of combined finite-difference schemes of high accuracy*, Dokl. Math., **97**:1 (2018), 77–81.
[28] N.A. Zyuzina, O.A. Kovyrkina, V.V. Ostapenko, *Monotone finite-difference scheme preserving high accuracy in regions of shock influence*, Dokl. Math., **98**:2 (2018), 506–510.
[29] M.E. Ladonkina, O.A. Neklyudova, V.V. Ostapenko, V.F. Tishkin, *Combined DG scheme that maintains increased accuracy in shock wave areas*, Dokl. Math., **100**:3 (2019), 519–523.
[30] O.A. Kovyrkina, V.V. Ostapenko, *On accuracy of a MUSCL type scheme when calculating discontinuous solutions*, Math. Models Comput. Simul., **13**:5 (2021), 810–819.
[31] O.A. Kovyrkina, A.A. Kurganov, V.V. Ostapenko, *Comparative analysis of the accuracy of three different schemes in the calculation of shock waves*, Math. Models Comput. Simul., **15**:3 (2023), 401–414.
[32] M.D. Bragin, O.A. Kovyrkina, M.E. Ladonkina, V.V. Ostapenko, V.F. Tishkin, N.A. Khandeeva, *Combined numerical schemes*, Comput. Math. Math. Phys., **62**:11 (2022), 1743–1781.
[33] S. Chu, O.A. Kovyrkina, A. Kurganov, V.V. Ostapenko, *Experimental convergence rate study for three shock-capturing schemes and development of highly accurate combined schemes*, Numer. Meth. Part. Diff. Eq., **5** (2023), 1–30.
[34] V.V. Rusanov, *Third-order accurate shock-capturing schemes for computing discontinuous solutions*, Dokl. Akad. Nauk SSSR., **180**:6 (1968), 1303–1305.
[35] S.Z. Burstein, A.A. Mirin, *Third order difference methods for hyperbolic equations*, J. Comput. Phys., **5**:3 (1970), 547–571.

[36] P.D. Lax, B. Wendroff, *Systems of conservation laws*, Comm. Pure and Appl. Math., **13** (1960), 217–237.
[37] P.D. Lax, *Hyperbolic systems of conservation laws and the mathematical theory of shock waves*, Philadelphia: Soc. Ind. Appl. Math., 1972.
[38] A. Harten, *On a class high resolution total variation stable finite difference schemes*, SIAM J. Numer. Anal., **21**:1 (1984), 1–23.
[39] A. Harten, J.M. Hyman, P.D. Lax, *On finite-difference approximations and entropy conditions for shocks*, Comm. Pure and Appl. Math., **29** (1976), 297–322.
[40] V.V. Ostapenko, *On the strong monotonicity of non-linear difference schemes*, Comput. Math. Math. Phys., **38**:7 (1998), 1119–1133. Zbl 0964.65084
[41] X. Liu, E. Tadmor, *Third order nonoscillatory central scheme for hyperbolic conservation laws*, Numer. Math., **79** (1998), 397–425.
[42] K.O. Friedrichs, P.D. Lax, *Systems of conservation equation with convex extension*, Proc. Natl. Acad. Sci: USA **68** (1971), 1686–1688.
[43] A. Harten, B. Engquist, S. Osher, S. Chakravarthy, *Uniformly high order accurate essentially non-oscillatory schemes, III*, J. Comput. Phys., **71** (2) (1987), 231–303.
[44] R. Courant, K. Friedrichs, H. Lewy, *On the partial difference equations of mathematical physics*, IBM Journal of Research and Development, **11**:2 (1928), 215–234.
[45] Y.I. Shokin, N.N. Yanenko, *The method of differential approximation (application to gas dynamics)*, Novosibirsk: Nauka, 1985. (in Russian)
[46] G. Strang, *Accurate partial difference methods II. non-linear problems*, Numer. Math., **6** (1964), 37–46.
[47] O.A. Kovyrkina, V.V. Ostapenko, V.F. Tishkin, *On convergence of finite-difference shock-capturing schemes in the regions of shock waves influence*, Dokl. Math., **504** (2022), 42–46.
[48] O.A. Kovyrkina, V.V. Ostapenko, *Monotonicity of the CABARET scheme approximating a hyperbolic system of conservation laws*, Comput. Math. Math. Phys., **58**:9 (2018), 1435–1450.
[49] B.S. Wang, W.S. Don, N.K. Garg, A. Kurganov, *Fifth-order A-WENO finite-difference schemes based on a new adaptive diffusion central numerical flux*, SIAM J. Sci. Comput., **42**:6 (2020), A3932–A3956.

Olyana Aleksandrovna Kovyrkina
Lavrentyev Institute of Hydrodynamics of SB RAS,
Lavrentyev Prospect, 15,
630090, Novosibirsk, Russia
Email address: kovyrkina.o.a@hydro.nsc.ru

Vladimir Viktorovich Ostapenko
Lavrentyev Institute of Hydrodynamics of SB RAS,
Lavrentyev Prospect, 15,
630090, Novosibirsk, Russia
Email address: ostigil@mail.ru